Climatic and environmental history of the past 1700 years recorded in the sediments of Laguna Espejo (39˚S) south-central Chile.

Master's Thesis

Faculty of Science

University of Bern

presented by

Patricia Alejandra Jana Pinninghoff

2014

Supervisor:

Prof. Dr. Martin Grosjean

Geographical Institute and Oeschger Centre for Climate Change Research

Co-Supervisor:

Dr. Iván Hernández Almeida

Geographical Institute and Oeschger Centre for Climate Change Research

Laguna Espejo, Patricia Jana Pinninghoff 2013

Laguna Espejo, Patricia Jana Pinninghoff 2013

Laguna Espejo, Patricia Jana Pinninghoff 2013

Table of Contents

List of Figures

List of Tables

Summary

South America is especially suitable for climate reconstructions because it is the only continuous landmass in the Southern Hemisphere spanning from northern to southern high latitudes. Geographically, there is an absence in climatic records from lake sediments around 40°S. This area is important due to its location in the transition zone between the westerly winds and the South Pacific anticyclone. Besides climate change, anthropogenic land-use changes are also of great concern. Southern Chile was affected by European settlement at the end of the 19th century, a process that resulted in the destruction of the forest do to use the land for agriculture.

This Master Thesis aims to distinguish between natural climate variability and anthropogenic changes in the sediments of Laguna Espejo (39°59'47.7" S; 72°10'29.21" W). Laguna Espejo is a maar lake located in the Chilean central valley. The main climatic influences are: El Niño Southern Oscillation, Pacific Decadal Oscillation, and the Antartic Oscillation, while the main activities in this area are agriculture, consisting mainly of wheat crops, *Pinus radiata* plantations and cattle. A non-varved lake sediment core taken in January 2013 was dated using ^{210}Pb and ^{14}C measurements. The sediment core was then analysed with non-destructive proxies: magnetic susceptibility; γ-bulk density, X-ray fluorescence, and hyper-spectral imaging. The destructive proxies included: water content, dry density, biogenic silica, grain size, total organic carbon and total nitrogen. A principal component analysis (PCA) and clustering were applied to reduce the data set and search for which forcing had a major influence in the sediments (climate / anthropogenic / volcanic). A multi-correlation analysis was performed between the proxies and the climate re-analysis records (temperature and precipitation) to search for a climate signal. Potential sources of the tephra layers were identified by examining records of historical eruptions from surrounding volcanoes.

The age-depth model was build using ^{210}Pb, historical settlement dates and ^{14}C measurements, giving the oldest age of 1700 cal. BP. Through characteristic peaks associated with volcanic origin elements in X-ray fluorescence was possible to identify four tephra layers. There is a change in every measured proxy in the sediment core between 33 and 13 cm that corresponds to the years 1882 and 1940 AD, respectively. This change is likely associated with the clearance of the forest by European settlers in the Laguna Espejo basin. After 1940 AD, the government began reforestation measures, which helped to reduce soil erosion around the lake, as evidenced in the measured proxies. However, total organic carbon and nitrogen increased from 1985 until the present. These increases are associated with more eutrophic conditions in the lake, due to a higher nutrient input into the lake by agricultural practices in the basin. The selected calibration period to identify the climate signal was between 1940 and 2009. To separate eutrophic signal from climate signal a PCA was performed for the calibration period. The PCA had one significant principal component, which means that the 20th century changes caused by European settlers had a much greater impact in Laguna Espejo sediments and overshadow the climate signal.

1. Introduction

1.1. Research motivation and state of the art

Climate change is a global concern (IPCC 2013). Anthropogenic activities since the 18th century have led to an increase in atmospheric CO_2 that, in consequence, increased the global temperature. Distinguishing between natural climate variability and anthropogenic forcing is an issue, especially because instrumental records are only available for the industrialization period (IPCC 2013). Using paleolimnological investigation, is possible to reconstruct climate at longer time scales, which helps to understand natural climate variability and the history of anthropogenic impact.

Mann et al. (2008) made a global climate reconstruction using different archives from around the world. Due to the lack of archives in the Southern Hemisphere, the reconstruction focused mainly on Northern Hemisphere temperature. Thus, it exists a need for high quality records from the Southern Hemisphere. South America is especially suitable for climate reconstructions because is the only continuous landmass in the Southern Hemisphere that spans the Equator to 55°S. Neukom et al. (2011) made a climate reconstruction using records from southern South America. In this study, only one record from lake sediments was used. However, lake sediments are highly suitable for climate reconstructions because they usually record long time periods and have a multi-proxy approach.

Besides climate change, anthropogenic impact by land use changes are also of great concern. The needs to generate space for agriculture lead to widespread forest clearance and intensive agriculture practices (crops and livestock; FAO 2006). This caused land degradation, increase in erosion rates and water eutrophication due to an excess of nutrient inputs (FAO 2006). In the Americas, this problem started with the arrival of the European colonizers in the 16th century.

In southern Chile, soil degradation was a main concern after the arrival of European settlers at the end of the 19th century (Otero 2006; Torrejón and Cisternas 2002) due to the European economic crises at the time. The settlers were obliged by the Chilean government to clear at least 1 Ha per year, which had negative consequences for the Chilean landscape, as around 40 % of the soil was eroded (Otero 2006).

Lake sediments record a mixture of environmental signals. There are two major sources of particle inputs to the lake: autochthonous and allochthonous. The autochthonous component corresponds mainly to biological detritus that is deposited in the sediment after the end of each organism's life-cycle. Some examples of these communities are: chironomids, diatoms, and chrysophyceas (Battarbee 2010; Smol 2008). The allochthonous material can reach the lake in several ways: (1) through soil runoff, where the inorganic and organic components of soils reach the lake; (2) through air dispersion, where volcanic fly ashes, as well as radionucleids, pollen, and other air particles are deposited in the lake through dry and wet deposition and then settled down by gravity; (3) through aquifers incorporating nutrients and minerals (Smol, 2008).

The advantage in use lake sediment records is than the register many signals from the basin and surroundings, like land-use changes, volcanic eruptions, and climate change. The disadvantage is that it is not always possible to separate these signals (McWethy et al. 2010). Thus, the challenge of paleolimnological studies is to distinguish and separate the different signals recorded in the lake sediments using statistical tools.

Most of the climate studies in Chile using lake sediments are qualitative. These studies use biological and geochemical proxies to identify changes in humidity (dry/wet) and temperature (cold/warm) during the Holocene (Fletcher and Moreno 2012; Urrutia et al. 2010; Bertrand et al. 2008). Nevertheless, von Gunten et al. (2009a) made a successful climate reconstruction of the last 800 years in central Chile (33°S) using chlorin content in sediments. In addition, Elbert et al. (2012) reconstructed the last 500 years of temperature in southern Chile (47°S) using biogenic silica. Both studies assumed that the limiting factor controlling *chlorophyll-a* and primary production in these two particular lakes was temperature.

1.2. Main aim and research questions

Geographically, there is a gap of climatic records from lake sediments at 40°S. This area is important due to its location in the transition zone between the westerly winds and the South Pacific anticyclone. This territory was also affected by European settlement at the end of 19th century. Another influence on this area is volcanic activity (Fontjin et al. 2014), as more than forty volcanoes have been active here during the Holocene.

The aforementioned reasons led to the research questions presented by this Master Thesis. The chosen study site is a lake called “Laguna Espejo”, located in south-central Chile (39°S). The research questions are as follows:

1. **Is it possible to separate the climate signal from the anthropogenic signal in Laguna Espejo? And, if possible, can this be used to make a climate reconstruction for the sediments of Laguna Espejo?**
2. **Is it possible to identify indicators of volcanic activity in the Laguna Espejo sediments?**

1.3. Project design

In order to answer the research questions and achieve the goals of this Master Thesis, the project was designed as follows:

1. **Retrieval of a sediment core:** A sediment core from Laguna Espejo was retrieved from the deepest point of the lake. This coring site was selected as the most representative of the lake (Smol 2008).
2. **Analysis of the core:** a 1 m long sediment core was dated and analysed for a series of physical and geochemical proxies. These proxies can be divided into non-destructive and destructive methods. The non-destructive methods were: magnetic susceptibility; γ-bulk density, X-ray fluorescence, and hyper-spectral imaging. The destructive methods were: water content, dry density, biogenic silica, grain size, total organic carbon and total nitrogen.
3. **Statistical analysis and comparison with climatic reanalysis data:** Principal component analysis was applied to reduce the data set. Together with a clustering analysis, they were used to search which forcing: climate, anthropogenic, and/or volcanic have an influence in which proxies along the core sediments. Finally, the proxies were compared with climate reanalysis data from the last century in order to search a climate signal by using a multi-correlation technique.

2. Study Site

2.1. General description of Región de la Araucania

Geological and tectonic setting

Región de la Araucania (Araucania from now on) is divided into three main geographical features (from West to East): the Nahuelbuta range, the central valley and the Andes range. These features resulted from the subduction of the Nazca Plate (oceanic) under the South American Plate (continental) (Pankhurst and Hervé, 2007; Stern et al. 2007). As result of the subduction process, the Central-Southern Volcanic Zone (CSVZ) was formed in the Andes range between the middle to late Pliocene and Pleistocene (Stern et al. 2007). The CSVZ is the most volcanically active segment of the whole Andes range and includes two of the most active volcanoes in South America: LLaima and Villarrica (Figure 1) (Stern et al. 2007).

Climate influences

The Andes range acts as an orographic barrier for the humidity carried by the westerlies during July (austral winter), which influences the climate of Araucania. The winter precipitation can reach up to 150 mm $month^{-1}$ (Figure 2a). During the austral summer, the precipitation is controlled by the anticyclone of the South Pacific (high pressure system) and the precipitation regimes can reach up to 30 mm $month^{-1}$ (Figure 2b) (Garreaud et al. 2009).

The main climatic anomalies that influence the precipitation and temperature in Araucania are: El Niño Southern Oscillation (ENSO) and The Pacific Decadal Oscillation (PDO) (Garreaud et al. 2009). The ENSO controls most of the interannual rainfall and temperature with a frequency between two to seven years (Garreaud et al. 2009). In the Pacific coast between the 35 °S and 40 °S, its positive mode (El Niño) is an anomaly of high temperatures and heavy precipitations during the Austral spring (Montecinos et al. 2000). On the contrary, its negative mode (La Niña) is characterized by colder temperatures and low precipitation during spring (Montecinos et al. 2000). The PDO is an ENSO-like event, but with different frequency and intensity. The frequency of PDO is every ten years and affects less than the 10 % of the year-to-year variance of precipitation and temperature. Thus the stronger effects occur when ENSO overlaps with PDO (Garreaud et al. 2009).

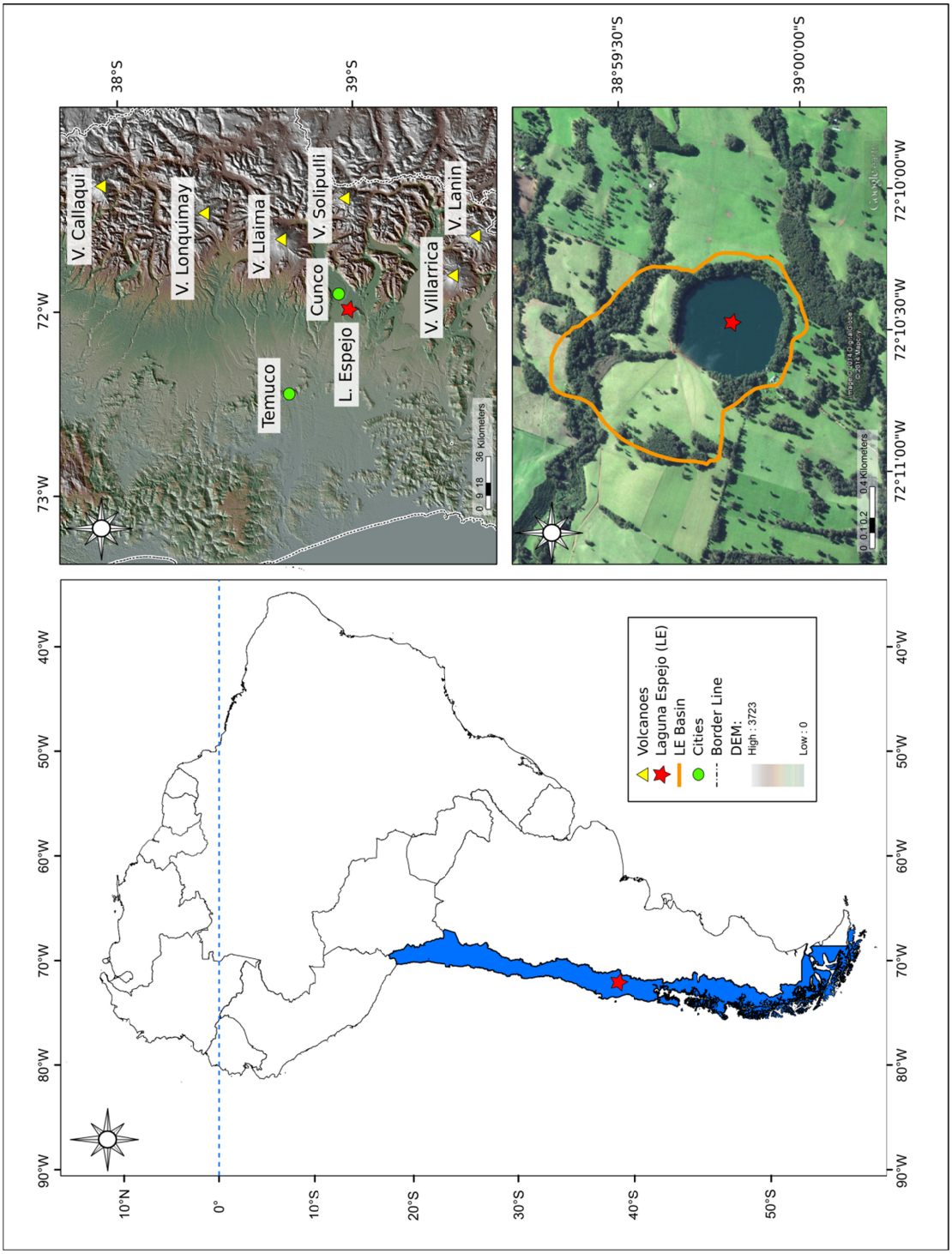

Figure 1: Overview map of the study area. Location of Chile and Laguna Espejo in South America (*left)*; Laguna Espejo with the surrounding volcanoes and cities (*top right)*; Basin of Laguna Espejo (*bottom right*).

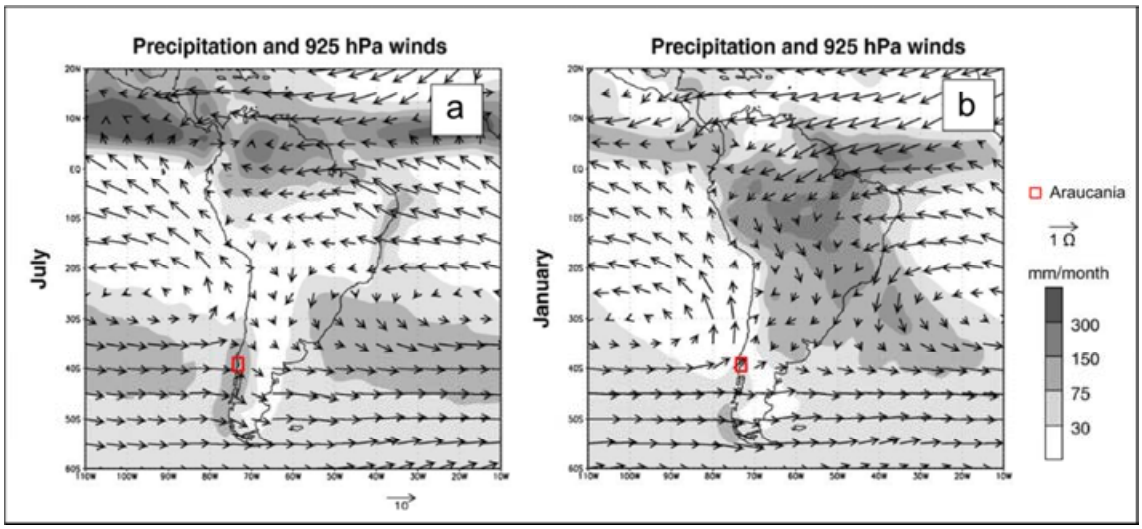

Figure 2: Precipitation and 925 hPa wind direction for (a) July (austral winter) and (b) January (austral summer) (from Garreaud et al. 2009).

Settlement process in the Araucania

Araucania was a territory populated by the Chilean indigenous people, called Mapuche, until the end of the 19th century (Torrejón and Cisternas 2002). The main activity of the Mapuche was agriculture (Torrejón and Cisternas 2002; Dillehay 1990). The main crops cultivated were maize (*Zea sp.*), potato (*Solanum tuberosum*), lima beans (*Vicia faba*), pumpkins (*Cucurbit sp.*), chilli (*Capsicum annuum*), quinoa (*Chenopodium quinoa*), and strawberry (*Fragraria chiloensis*) and the raising of llama (*Lama sp.*) (Dillehay 1990). The Chilean Government started an European colonization program in the southern territory during the middle of the 19th century. In Araucania, the settlement process started in the year 1882 AD (Otero 2006). Higher food demands led to land clearing and forest loss for crops and/or livestock. Due to the lack of technology, the settlers used the technique of burning the forest (Otero 2006), which was accepted and promoted by the government until the creation of the Forestry Department in 1957. The Forestry Department had the mission to start a forest protection program (Otero 2006). Since then, the conservation of native forest is promoted by the state, and forest fires are strictly prohibited.

2.2. Laguna Espejo

Laguna Espejo (39°59'47.7" S; 72°10'29.21" W and 348 m.a.s.l.) is located in Araucania at 50 km east Temuco and 15 km west Cunco (Figure 1). As previously mentioned, this region is known to be a highly active volcanic area. The main active volcanos near Laguna Espejo are: Volcán Callaqui (37.9° S, 71.4° W), Volcán Lonquimay (38.3° S, 71.4° W), Volcán Llaima (38.6° S, 71.6° W), Volcán Solipulli (39.0° S, 71.5° W), Volcán Villarrica (39.5° S, 71.9° W), and Volcán Lanin (39.6° S, 71.5° W) (Figure 1). The main activity in this area is agriculture, mainly wheat crops, *Pinus radiata* plantations and cattle.

Laguna Espejo is a maar lake, formed after a volcanic eruption. Its geological setting is defined as partially weathered Pliocene-Pleistocene volcanic centres and sequences: mainly basaltic lavas with tuffs interbedded (SERNAGEOMIN 2003). The basin of Laguna Espejo is flat and its area is 1.4 km^2. The maximum water depth is ~38 m and the lake area is ~0.5 km^2. The seismic profile shows up to 15 m of sediment thickness (Figure 3). Laguna Espejo has very steep walls and a flat bottom (Figure 3).

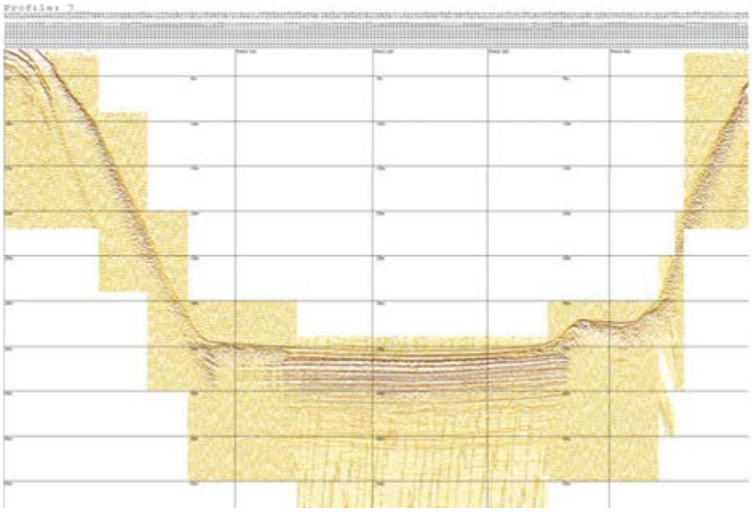

Figure 3: Seismic profile of Laguna Espejo (Abarzúa 2010)

Laguna Espejo is fed by ground water, rain-fall, and water runoff. Laguna Espejo is a warm monomictic lake, which means that the lake is mixed once a year during winter. At the time of fieldwork (austral summer) the water was stratified (Figure 4). The epilimnion depth was 5 m and the temperature, conductivity, and dissolved oxygen (DO) were 28 °C, 60 µS cm^{-1}, and 108 %, respectively, and the pH decrease from 7.3 to 6.8 in the first 0.5 m and then increases until 7.0 through the epilimnion (Figure 4). The metalimnion was located between 5 and 10 m depth. Here the temperature, and conductivity, decrease from 15 to 10 °C, and from 60 to 53 µS cm^{-1}, respectively. On the contrary, the DO had two peaks at 6 and 9 m of 121 and 136 %, respectively, and the pH increased from 7.0 to 7.9 (Figure 4). The hypolimnion was below 10 m depth and the four variables decrease. The temperature decreases from 15 to 10 °C, the conductivity from 53 to 49 µS cm^{-1}, the DO from 136 to 100 %, and the pH from 8.0 to 7.5 (Figure 4).

There are three types of vegetation around Laguna Espejo: native and exotic forest, and crops. The native vegetation in this zone is classified as the deciduous forest of the central valley (Gajardo, 1994). The main species are *Laureliopsis philippiana, Nothofagus obliqua* and *Nothofagus dombeyi*. The exotic vegetation is used as forest resources and as ornamental plants, and sometimes they are mixed with the native forest. The exotic species are mainly *Pinus radiata* and *Eucalyptus globulus*. The crops are part of the farming activities in the surroundings of Laguna Espejo. These are mainly wheat and oats.

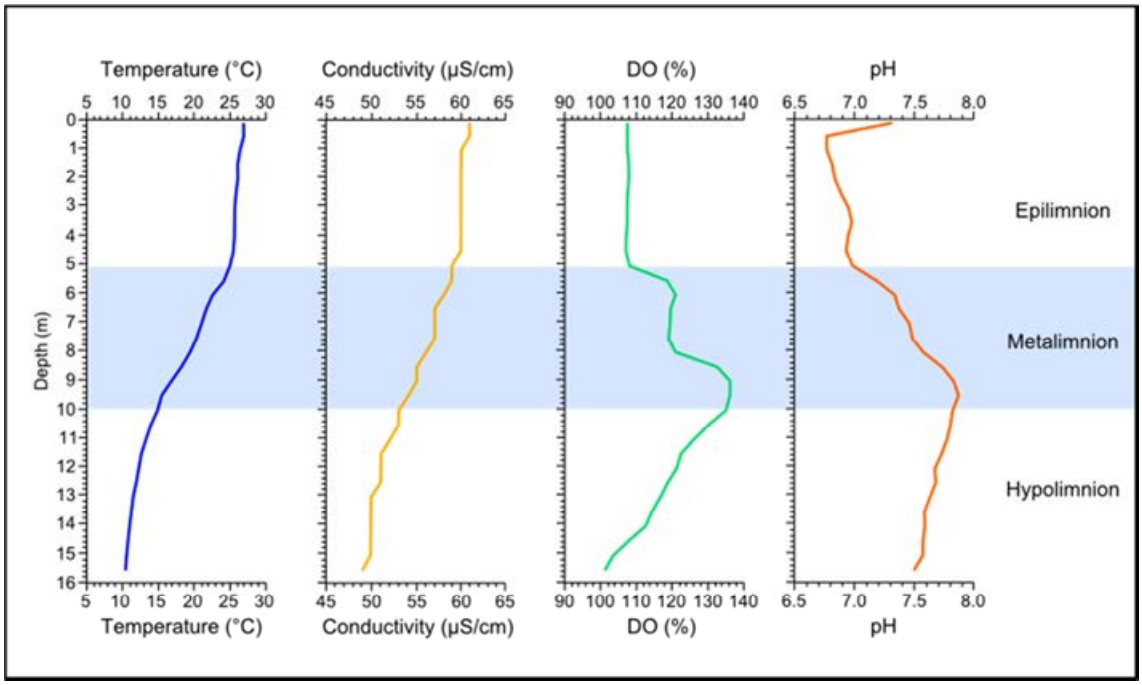

Figure 4: Physical parameters of the first 15.5 m of the water column in Laguna Espejo measured on January 28th, 2013. From left to right: temperature, conductivity, dissolve oxygen (DO) and pH.

3. Material and Methods

3.1. Sampling

Four sediment cores were taken from Laguna Espejo in January 2013 using an Uwitec gravity corer. Two cores were taken near the shore (LE13-1 and LE13-4; Figure 5.1) and the other two were taken at the deepest point of the lake (LE13-2 and LE13-3; Figure 5.1). The cores were sealed and stored in a cold chamber at 4 °C in order to avoid oxidation and diagenetic biological processes. After one month, they were sent by plane to the Lake Sediments and Paleolimnology laboratory of the University Bern (Switzerland) to be analysed.

3.2. Core analyses

Figure 5 shows the procedures followed in order to acquire the data. First, the four cores extracted from Laguna Espejo (LE13-1 of 96.5 cm long, LE13-2 of 95.6 cm long, LE13-3 of 95.2 cm long, and LE13-4 of 71.5 cm long; Figure 5.1) were analysed for the physical properties: magnetic susceptibility (MS) and γ-bulk density. After this, all cores were split into two halves (A and B) and scanned for hyper-spectral image analysis. As LE13-2 was the longest core taken from the deepest point, it was chosen as master core. Thus, the LE13-2 core was scanned using X-ray computed tomography (CT), X-ray fluorescence (XRF) (LE13-2B) and a detailed stratigraphic description was performed (LE13-2B) (Figure 5.2).

After the scanning processes, both halves of the core LE13-2 were sub-sampled. First, core LE13-2A was sub-sampled by taking 1 cm^3 of sediments with 1 cm resolution along the core. These samples were analysed for dry density and water content. The chronology was established by ^{210}Pb and ^{137}Cs dating every 0.5 cm for the top most 20 cm of the core, the starting of the settlement process in 1982 at the 33 cm, and AMS ^{14}C dating of bulk sediments on four samples downcore (Figure 5.3).

The core LE13-2B was sub-sampled every 0.2 cm for the first 34 cm. These samples were analysed for total organic carbon (TOC), total nitrogen (TN), and grain size along 34 cm, and biogenic silica (bSi) only for the uppermost 20 cm. Between the 34 and 95.6 cm the core was sub-sampled every 1 cm, excluding the volcanic tephra identified by visual inspection. For these samples, TOC, TN and grain size were analysed (Figure 5.4).

After the core analysis (Figure 5.5), the proxies were correlated to climate variables (precipitation and temperature). If the data have a climate signal, this can be used for climate reconstructions (Figure 5.6). In parallel, an environmental reconstruction was performed (Figure 5.7).

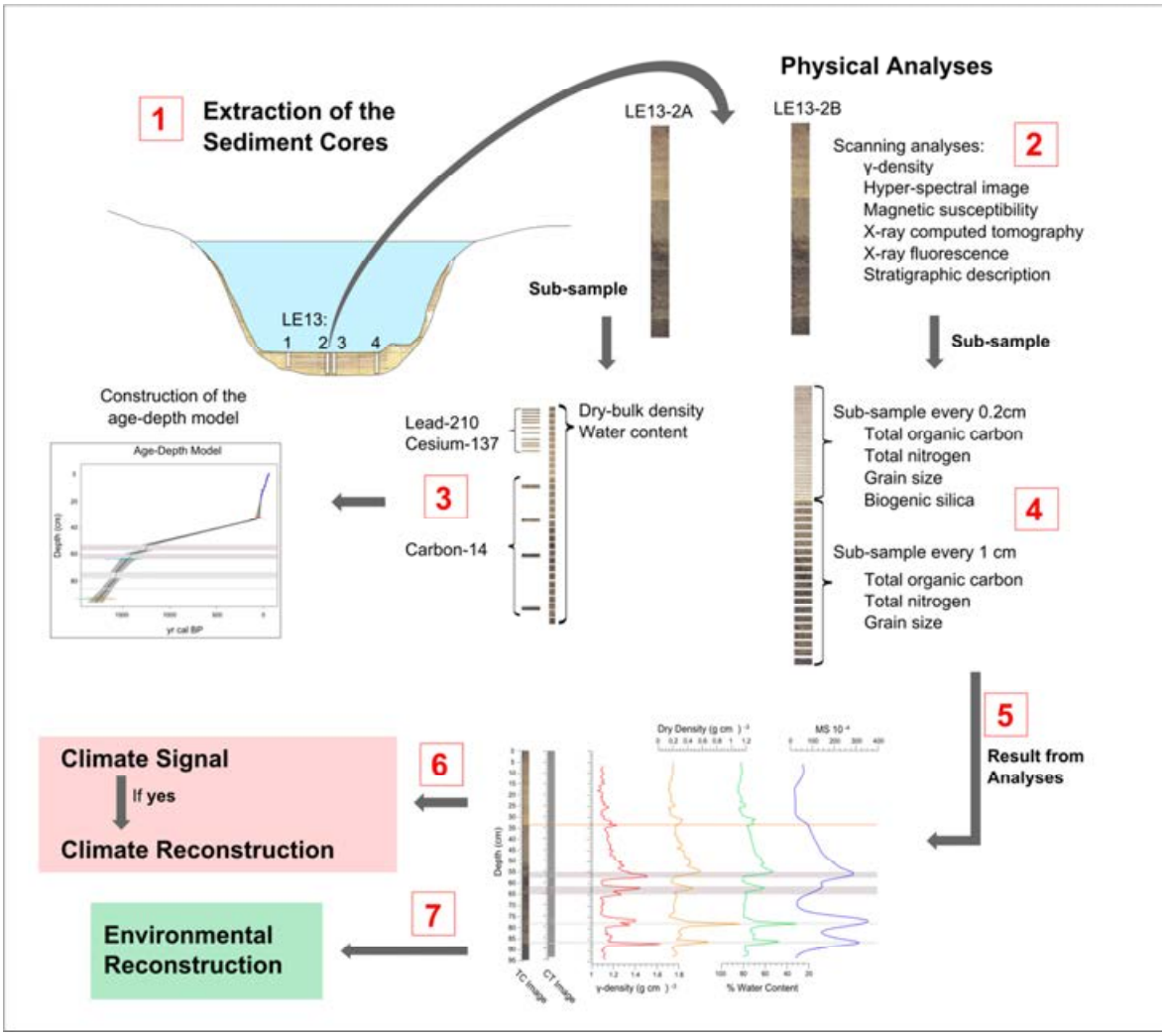

Figure 5: Representation of the methodological procedures (adapted from Smol 2008). (1) Extraction of the sediment cores from Laguna Espejo. (2) Scanning analyses performed on LE13-2 core. (3) Sub-sampling of core LE13-2A for the age-depth model construction and dry density and water content analyses. (4) Sub-sampling of core LE13-2B for destructive-physical analyses. (5) Results from analyses. (6) Search for climate signal and possible climate reconstruction. (7) Environmental reconstruction.

3.2.1. Dating

^{210}Pb

^{210}Pb is a radioisotope that comes from the decay chain of ^{238}U. There are two components of ^{210}Pb in lake sediments, the supported and unsupported ^{210}Pb. Supported ^{210}Pb ($^{210}Pb_s$) is produced in-situ and its production is in equilibrium with the system. The unsupported ^{210}Pb ($^{210}Pb_u$) reaches the lakes through the atmosphere and soil runoff. This process occurs because the ^{226}Rn in the soil decays into ^{222}Rn, which volatilizes to the atmosphere and quickly decays into $^{210}Pb_u$, precipitating into the lake and later incorporated to the lake sediments. As the production of $^{210}Pb_u$ fraction is not in equilibrium with the system, then is used to date the sediments (Appleby and Oldfield 1978).

For LE13-2B, eleven samples of 0.5 cm thick were sent to Flett Research Ltd laboratory. The total ^{210}Pb (^{210}Pb$_t$) activity was determined indirectly by the measurement of its alpha-emitting granddaughter nuclide ^{210}Po. In order to obtain the ^{210}Pb$_s$, three samples were measured for ^{226}Ra. Then the ^{210}Pb$_u$ was calculated as shown in Equation 1.

$$^{210}Pb_u = {}^{210}Pb_t - {}^{210}Pb_s$$

Equation 1 (Appleby and Oldfield 1978)

It is necessary to apply a model in order to transform the ^{210}Pb$_u$ activity to numerical ages (years after deposition). The most used models are the "constant initial concentration" (CIC) and the "constant rate of supply" (CRS) (Arnaud et al. 2006; Appleby and Oldfield 1978). The most suitable model would be the one that is most consistent with other chronological markers in the profile like ^{137}Cs (von Gunten et al. 2009b).

^{137}Cs

As it was mention before, additional markers are needed in order to improve the dating model. One of these stratigraphic markers is the maximum fall out of ^{137}Cs, produced by nuclear weapons test during the ending of the 1950s and the beginning of the 1960s. The maximum fall out peak of ^{137}Cs is established at 1963 for the Northern Hemisphere (Cohen 2003) and at 1965 for the Southern Hemisphere (Arnaud et al. 2006). One problem of the ^{137}Cs is that it can be diffused through the sediment column, which could result in the absence of the maximum fallout peak (Cohen 2003), especially in Southern hemisphere, where the concentrations of ^{137}Cs are low.

^{14}C

^{14}C is the unstable isotope of carbon. ^{14}C is formed by interaction of cosmic ray spallation products with stable ^{14}N gas in the highest atmosphere. The cosmic rays take away a proton from ^{14}N forming the ^{14}C that quickly oxidises to $^{14}CO_2$ and it is incorporate to the plant and animal life through photosynthesis and to the food chain. When the organisms die, the ^{14}C stops to be in equilibrium and starts to decay with a half-life time of 5730 years.

There are several problems with ^{14}C dating. One of these problems is that the age of deposition of the sample may not be the same as the age of the sample. Older carbon can reach the sediments through soil erosion and secondary transportation. This process is known as reservoir effect. Lakes with long residence times usually have larger reservoir effect. These lakes can retain the dissolved inorganic carbon (DIC) for a long time, which later precipitates and is incorporated into the sediment, which makes the sediment older. The reservoir effect can be avoided by using terrestrial organic matter, especially terrestrial plants, because these assimilate the carbon from atmospheric CO_2 (Cohen 2003).

The concentration of ^{14}C in the atmosphere has not been constant through time. In consequence, a calibration curve was made using tree rings, which are different for each hemisphere. The last calibration curve made for the Southern Hemisphere is SHCal13 (Hogg et al. 2013), which was used

for the calibration of the ^{14}C dates (cal. ^{14}C) of the sediment core LE13-2. Nuclear weapon tests, during the 1950s and 1960s, changed the concentration of ^{14}C in the atmosphere. Concequently, the ^{14}C ages are given in ages before 1950 or better known as ages before present (BP).

Seven samples for ^{14}C dating were taken from the LE13-2 core and were sent to the LARA AMS laboratory at the University of Bern. Four bulk sediment samples were taken at 33.5-34.5 cm, 44-45 cm, 64-65 cm, and 93.5-94.5 cm. Three leaf samples were taken from layers adjacent to where bulk samples had previously been sampled for dating; one at 64-65 cm and two leaves at 93.-94.5 cm. The bulk sediment samples were separated into three fractions of the organic matter: bulk organic fraction, alkali-soluble fraction or humic acid and alkali-insoluble fraction or humin (Cohen 2003).

Age-depth model

The age-depth model was built using the Clam 2.2 script (Clam from now on) (Blaauw 2010) implemented in R (R Core Team 2012). The Clam incorporates all the ages of the sediment core to perform the age-depth model, including ^{210}Pb ages and other age markers like historical ages. The script also includes the calibration curve for the Southern Hemisphere SHCal13. For LE13-2, it was incorporated the seven ^{210}Pb ages, the historical settling staring in 1882 AD at the 33 cm, and the ^{14}C dates from the three macrofossils. The setting used was the following: the curve for interpolation used was the `type 1` = "linear interpolation between neighbouring levels". The calibration curve used was the `cc3` = "SHCal13". The `outliers()` function was used for the bulk sediment samples from the 33.5 - 34.5 cm and 44.0 - 45.0 cm. The function `slump()` was used to remove the tephra layers from the age-depth model. The `dmax()` function was used to set the maximum depth extrapolation for the model. Then every function was used to set the resolution of the age-depth model. Finally, the `accrate=1` function was used to calculate the linear accumulation rate (LAR) in cm yr^{-1} (Blaauw 2010).

3.2.2. Physical analyses

Sediment classification and stratigraphic description

A detailed stratigraphic and sedimentological description of a sediment core is important for paleolimnological studies. Information gathered during visual description of the cores helps to understand past environmental dynamics as well as facilitates studies of lacustrine facies modelling (Schnurrenberger et al. 2003). The classification in the LE13-2 core was performed by following the method described in Schnurrenberger et al. (2003). Four criteria were used for the core description. First, the core was divided into different units that were defined by identifying colour with a Standard Munsell soil colour charts (Munsell Colour Company 1994) and/or structure changes along the core. The second classification criterion was the lithology. The sediment was classified as gravel, sand/detrital, silt/clay/detrital, carbonate, evaporites, peat/organic, and/or volcanic ash. A test for hydrochloric acid (HCl) reaction was performed on the 8, 23, 41, 52, 55, 61, 64, 71, 78, 82, 87, and 91 cm to test the presence of inorganic carbon in the sediment. The third criterion was the contact of the different sediment units, which could be sharp (less than 2 mm), gradual (between 2 and 10

mm), wavy, or erosional. The fourth criterion was the texture of the sediment, referring if the sediment core was laminated, banded, massif/granular, porphyric, platy, “mottled flames”, graded, or bioturbated.

X-ray computed tomography

The CT is a non-destructive scanning technique that indicates allows the visualization of the internal structure of the sediment core and thus, makes it possible to recognize structures like tephra layers. The CT scanner uses the atomic composition and variation in density of the sediments in order to produce continues 3D images of the sample (Mees et al. 2003). The scan was performed on a CT scanner (Siemens Somatom 6) from the Institute of Forensic Medicine at the University of Bern. The X-ray energy was set at 110 keV with a tube current of 100 mA. The slice resolution was 1.25 mm with an increment of 0.6 mm. The field of view was 75 mm with a matrix of 512 x 512 pixels and the collimation was 6 x 0.5 mm.

Magnetic susceptibility

The MS is a non-destructive technique that measures the degree of magnetization of a material in response to an applied magnetic field. The MS in the LE13-2 core was measured with a Geotek Multisensor Core Logger (MSCL) in the Geology Department at the University of Bern. The resolution was 0.5 cm, but the magnetic field had an influence of 5 cm. High values of MS can reflect an increase of soil erosion and volcanic tephra layers. These events supply more mineralogical particles and magnetic minerals to the lake (Sandgren and Snowball 2001).

γ-Bulk density

The principle of this method consists of measuring the bulk density reflected by the combined effect of variations in porosity, grain density (dominant mineralogy), and coring disturbance. The porosity is controlled mainly by lithology, texture, compaction, and cementation (by both mechanical and chemical processes). Therefore, variations in γ-bulk density may reflect variations in the accumulation rates or concentrations of sands, gravel, and/or clays (Zolitschka et al. 2001). As well as with the MS, the γ-bulk density analysis of the LE13-2 core was made with the Geotek MSCL in the Geology department at the University of Bern with a measurement resolution of 0.5 cm.

Reflectance spectroscopy analysis

The chlorins (*chlorophyll-a* diagenetic products) content were measured using two reflectance spectroscopy-analysis techniques. The first technique consists of scanning the sediment core with a Gretag-Spectrolino (GretagMcBeth, Switzerland). The calibrated reflectance spectrum was measured at 10 nm resolution between 380 and 730 nm. The measurement interval along the sediment core was 0.2 cm. This measurement was applied to the core LE13-3 because the Spectrolino deforms the surface of the core, which can alter other analysis performed on both halves of the master core LE13-2. The second technique consists of scanning the sediment core with a Specim Ltd hyper-spectral imaging scanner. The range of the reflectance spectra is between 400 and 1000 nm, with a spectral

resolution of 0.8 nm and a spatial resolution of 38 × 38 µm. The data normalization and analysis is made using remote sensing software (ENVI 5.0). As this is a non-destructive technique, the four cores from Laguna Espejo were scanned with the Specim Ltd. scanner.

After the scanning, the spectral index for chlorin content was calculated. As chlorins have their maximum absorption band between 660 nm and 670 nm, the relative absorption band depth ($RABD_{660;670}$) between these wavelengths was calculated (Figure 6). The $RABD_{660;670}$ (Equation 2), developed by Rein and Sirokco (2002), consists of projecting a theoretical line between the two maximums. The difference between this theoretical band and the maximum absorption depth is calculated (Figure 6). Thus, the larger is this difference, the higher the concentration of chlorins in the sediment (Rein and Sirockco 2002).

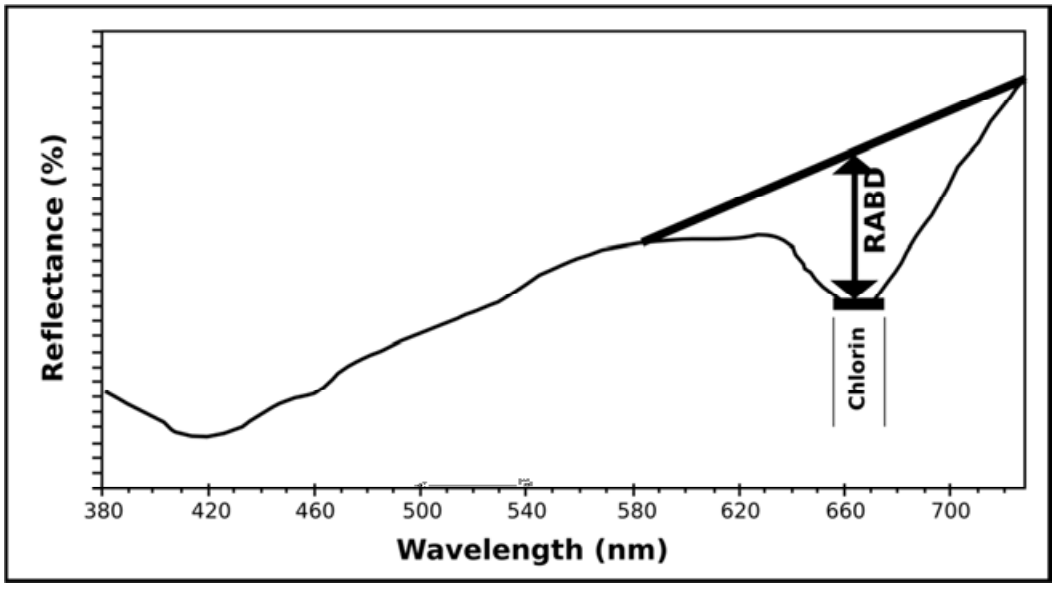

Figure 6: Relative absorption band depth ($RABD_{660;670}$) estimation for chlorins (Rein and Sirockco 2002).

$$RABD_{660;670} = ((6 \times R_{590} + 7 \times R_{730})/13)/R_{\min(660;670)}$$

Equation 2

3.2.3. X-ray fluorescence

XRF is a non-destructive technique for the estimation of the elemental composition of lake sediments. The XRF analysis is based on excitation of electrons by incident radiation that creates vacancies which are filled by electrons falling back from the outer shells. The excess energy produced is emitted as a pulse of secondary X-radiation fluorescence. The spectra, generated by this fluorescence energy and wavelength, are unique for the atoms of each element, which allows to estimate the relative abundance of the elements present in the sediment (Weltje et al. 2007). With XRF it is only possible to perform qualitative estimations of the different element abundances.

(Eq. 2) $RABD_{660;670}$ = Relative absorption band depth at 660 mn or 670 nm wavelength; R_{590} = Reflectance at 590 nm wavelength; R_{730} = Reflectance at 730 nm wavelength; $R_{min(660;670)}$ = Minimum reflectance between 660 nm and 670 nm wavelength.

Ti and K are components present in soil, specially found in clays (Vogel et al. 2010), and their changes in lake sediments are usually associated with aeolian and fluvial in-puts into the lake. In contrast, Zr is also a terrigenous element very resistant to chemical and physical weathering associated with larger grain sizes (Kylander et al. 2011). An increase in the count of these elements would be an indicator of soil erosion (Kylander et al. 2011; Vogel et al. 2010). On the other hand, Fe and Mn can be indicators of redox conditions. A more rapid reduction of Mn than Fe under anoxic conditions would lead to a preferencial Mn release, resulting in lower Mn/Fe ratios. As Fe oxidises faster than Mn, high Mn accumulation and thus, higher Mn/Fe ratios occurs under oxic conditions (Naeher et al. 2013; Cohen 2003). But Fe is not necessarily remobilised by redox changes and can also be tracer for terrigenous sources, specially when is correlated with K and Ti (Naeher et al. 2013). Br is an indicator of organic matter production in the lake (Hennekam and de Lange 2012). In the sediment core, Si can have two sources allochthonous and autochthonous. The allochthonous terrigenous material can be determined with a high positive correlation with Ti. The autochthonous Si is the biogenic Si (bSi) produced by diatoms, which is described in the next section. Finally, volcanic tephra layers can be identified by a peak in the following elements: Si, Ti, Fe, Mn, Zr, K, Rb, Sr and Ca (Naranjo and Stern 1998). Ca also can be either formed in the soil (i.e. Ca-feldspar) or in the lake (i.e. calcite). However since the calcite and Ca-feldspar are very susceptible to chemical weathering (Boyle 2001), Ca cannot be considered as an erosion proxy.

Laguna Espejo sediments were analysed with an ITRAX XRF Core Scanner at the Institute of Geological Sciences in the University of Bern. The elemental composition of lighter elements was measured with a cobalt tube and for heavier elements the measurement was performed with a chrome tube.

3.2.4. Biogenic silica

The bSi is related to the remains of siliceous phytoplankton (mainly diatoms). An increase of nutrient availability in the lakes, leads to an increase in the production of diatoms and, hence, an increase in bSi. Anthropogenic activities, like forest clearance, increase the availability of nutrients like phosphorous and hence the primary productivity in the lake increases (Conley and Schelske 2001).

For the bSi analysis, 100 samples were taken from the first 20 cm of the LE13-2B core. First 100 mg of freeze-dried and homogenized sample were placed into centrifuge tubes and 5ml of H_2O_2 (30 %) were added in order to oxidise the organic matter. After one week the samples were heated in a water bath for 1 h at 80 °C and centrifuged for 15 min at 3500 rpm. The supernatant was removed with a vacuum pump and the samples were washed with milli-Q water. After this, the samples were shook at 1500 rpm; they were put again in the centrifuge for 15 min at 3500 rpm. The excess of water was removed again and the samples were freeze dried.

For the bSi extraction, 10 ml of NaOH 1 M was added to each freeze dried sample and six blanks. The tubes were put into the ultrasonic bath for 1 min and after they were hand-shook and then put for 1 h into the oven at 90 °C. This process was repeated three times. The tubes were placed in the centrifuge for 15 min at 3500 rpm. A 1:100 solution was prepared for the measurement, which

consisted in to put 10 ml of milli-Q water, 14 µl of HNO_3 (65 %), 140 µl of the sample, and filled up the tubes until 14 ml with milli-Q water. For the measurement of the bSi, a Varian inductively coupled plasma optical emission spectrometry equipment was used. This equipment is located at the Paul Scherrer Institute (PSI). The remaining sediment was later used for grain size analysis.

3.2.5. Grain size analysis

Grain size distribution is a common technique in paleolimnology used to determine sedimentation processes (Smol 2008). The most common classification is the Wentworth grain size distribution (Table 1) that consists of separating the grain size lasses according to their size. In sediment cores, usually it is possible to distinguish three major classes: clay, silt and sand (Table 1).

The grain size analysis was performed all along the LE13-2B core with a Malvern Mastersizer 2000S that measures the entire range between clay and sand. For the first 20 cm, the remaining sediment from the bSi was used. Between 20 and 35 cm, the sediment was subsampled every 0.4 cm between the 20-35 cm and below 35 cm the subsamples were taken at 46.6, 53.2, 54.0, 60.0, 65.0, 76.5, and 85.5 cm.

In lake sediment cores, a high concentration of clay particles is usually interpreted as a signal of erision (Smol 2008; Van Hengstum et al. 2007). A larger particle size is usually related to a high-energy sedimentary environment related to an increase of river flows or precipitation (Smol 2008). Also, volcanic tephra layers usually are related to higher grain sizes (i.e. sand).

Table 1: Wentworth classification (from Lars 2001)

Limiting Particle Diameter			Descriptive Terms			
phi	mm	µm				
-11	2048		Very Large	Boulder		Gravel
-10	1024		Large			
-9	512		Medium			
-8	256		Small			
-7	128		Large	Cobble		
-6	64		Small			
-5	32		Very Coarse	Pebble		
-5	16		Coarse			
-3	8		Medium			
-2	4		Fine			
-1	2		Very Fine			
0	1	1000	Very Coarse	Sand		
1	0.5	500	Coarse			
2	0.25	250	Medium			
3	0.125	125	Fine			
4	0.0625	62.5	Very Fine			
5	0.03125	31.25	Very Coarse	Silt	Coarse	Mud
6	0.01563	15.63	Coarse		Medium	
7	0.00781	7.81	Medium		Fine	
8	0.00391	3.91	Fine		Very Fine	
9	0.00195	1.95	Very Fine	Clay	Clay	

3.2.6. Total organic carbon and total nitrogen

TOC is an indicator of productivity of the lake (Meyers and Teranes 2001). The organic matter in the water column sinks to the lake bottom and is buried in the sediments, where it can be preserved or degraded by organisms. The TOC measured in the sediment samples is considered to be proportional to the organic matter in the lake sediments (Cohen 2003).

The TOC/TN (C/N) ratio is used to determine the origin of the TOC. The main component of terrestrial plants is cellulose, which has a higher TOC content (Bertrand et al. 2010). On the contrary, the algae are rich in protein with a higher content of TN (Bertrand et al. 2010). Therefor C/N ratios >20 indicate allochthonous sources of TOC, and C/N ratios <10 indicates autochthonous source of TOC (Figure 7) (Meyers and Teranes 2001). Finally, values between 10 and 20 indicate a mixture between the two sources (Meyers and Teranes 2001).

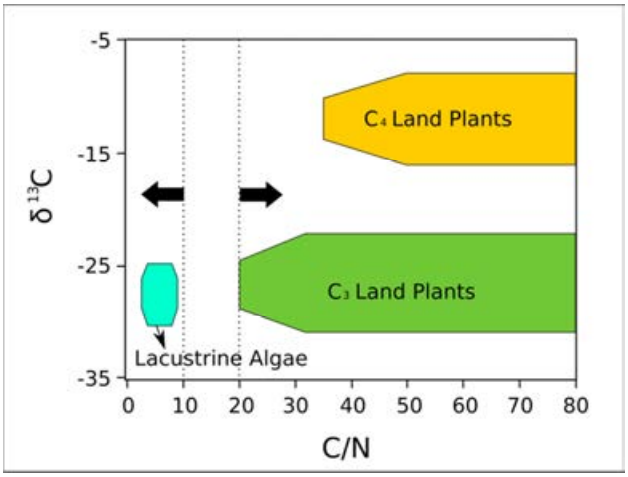

Figure 7: Representation of the elemental and $\delta^{13}C$ composition of organic matter from lacustrine algae, and C_3 and C_4 land plants (adapted from Meyers and Teranes 2001).

3.2.7. Statistical analyses

Statistical analyses are used to provide information about the structure and relationships of the sediment components. The statistical analyses performed to the whole LE13-2 data set were: principal component analysis (PCA), hierarchical and non-hierarchical cluster analyses, and correlation matrix.

The PCA uses the optimization of the variance-covariance matrix to classify the data. The number of principal components (PC) is as high as the number of variables included in the analysis. In order to determine the number of significant PC, a broken stick model was used. The different PCs represent different compositional assemblages in the sediment core with different sources. As an example, if two PCs are significant then one could be related to terrigenous material and the other to organic material in the lake.

Cluster analyses are used to categorize and split the data in groups of observations that are similar. This clustering can be hieratical or non-hieratical. Hierarchical methods start with the individual objects. The most similar objects are grouped, and these initial groups are merged according to their similarities. For this study, we used the constrained incremental sum-of-squares (CONISS). The non-hierarchical cluster consists in grouping the variables of k numbers of clusters. In this study we used the k-means cluster analysis (Jolliffe 1987). Finally, the correlation matrix contains the correlation coefficients for the variables, which allows the identification of the correlation among the different proxies.

3.3. Calibration and climate reconstruction

The Calibration-in-time (CIT) approach described by von Gunten et al. (2012) was followed in order to calibrate the proxy data to meteorological data. The time interval used to make the calibration is called calibration period. The CIT approach requires a good and high-resolution sediment chronology with small uncertainties and high-resolution proxies during the calibration period. The CIT is unique for each lake and the period that comprises the calibration period typically covers ca. 100 years (von Gunten et al. 2009a).

Long and regular time-series of instrumental climate data are rare in the Southern Hemisphere (von Gunten et al. 2009a). Due to the absence of adequate meteorological data we used the CRU TS 3.21 reanalysis data for temperature and precipitation extracted from http://climexp.knmi.nl (Trouet and van Oldenbourgh 2013). This reanalysis data covers the 1901 AD to 2009 AD period. The quality of the data was assessed by comparing reanalysed data with local instrumental-climate data. Also, a spatial correlation map for each meteorological variable was made in order to know the regional significance of this data.

The proxy data is irregular in time duration, so it needs to be regularised to annual resolution. To regularise the proxy data, it was interpolated to the same annual values of the meteorological data and then both, proxy and climate data were filtered at 3, 5 and 7 yr using a triangular filter. The proxy data were individually or combined as PC correlated (R pearson) with the meteorological data (von Gunten et al. 2012). The levels of significance were calculated (significant = p-value < 0.05), which were also corrected for autocorrelation in the time series (significant = $p_{corr} < 0.05$). The autocorrelation can be due to bioturbation or small data points in the calibration period, which reduces the likelihood of a good calibration (von Gunten et al. 2012). After the calculation of the significant correlation matrix it was necessary to check for “false positive” results (von Gunten et al. 2012). Finally, if there was a positive climate-proxy correlation the calibration model would be validated using a (k-fold) cross-validation method. The proxy was transformed to climate variable in order to make the climate reconstruction downcore (von Gunten et al. 2012).

4. Results and Interpretation

The four studied cores were taken along a transect from NW to SE in Laguna Espejo (Figure 8.a). The Figure 8.b shows the stratigraphic correlation between these four cores based on lithological changes. Five points could be correlated which are marked with the same colour and number. The first correlation (green arrow) is a very well-marked black line in cores LE13-1 and LE13-4 at 68 cm and at 37 cm, respectively. The second correlation (pink arrow) is Layer 1 (L1) (Figure 9), in which there is a drastic change of colour in the four cores before and after L1. L1 is at 75 cm in LE13-1, at 33 cm in LE13-2, and at 38 cm in LE13-3 and LE13-4. The third correlation (red arrow) is the tephra layer 4 (T4) (Figure 9). T4 is at 94 cm in LE13-1, at 54 cm in LE13-2, and at 56 cm in LE13-3. T4 is not present in LE13-4 core. The fourth correlation (orange arrow) is the tephra layer 3 (T3) (Figure 9). T3 is at 58 cm in LE13-2, and at 66 cm in LE13-3. Finally, the fifth correlation (purple arrow) is at 86 cm in both LE13-2 and LE13-3 (Figure 8.b). The core LE13-1 has the higher sedimentation rate between L1 and the top of the core. This could be because it receives more material from the area with no vegetation of the basin of Laguna Espejo (Figure 8.a).

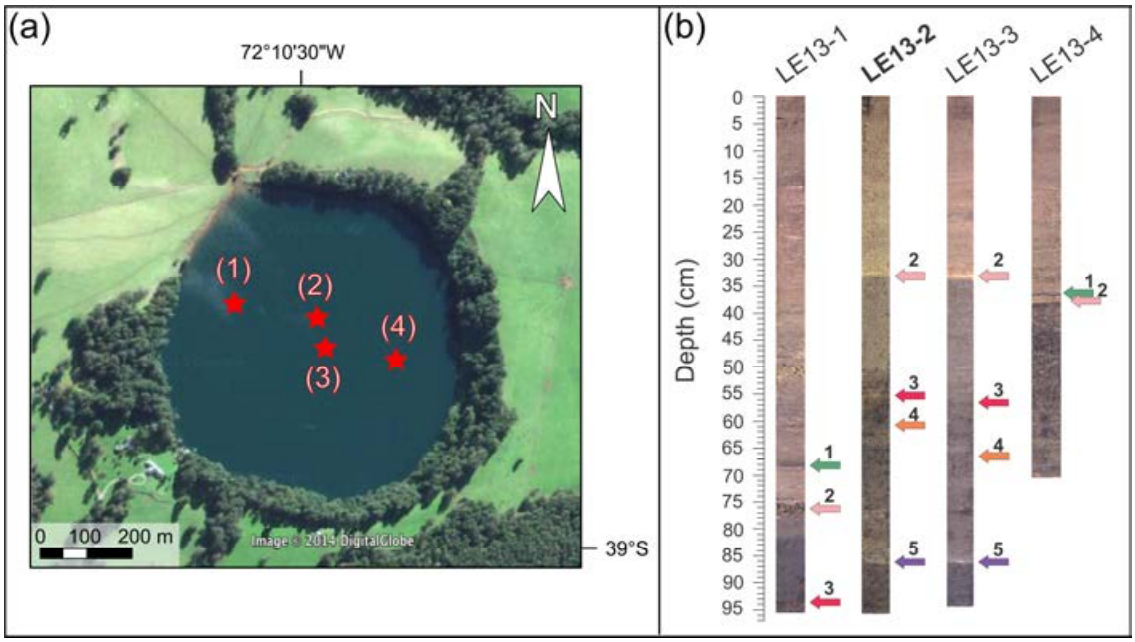

Figure 8: (a) Sampling sites for the four cores: (1) LE13-1; (2) LE13-2; (3) LE13-3; (4) LE13-4. (b) Stratigraphic correlation between the four cores from Laguna Espejo.

4.1. Master core (LE13-2) analyses

The hierarchical cluster was made using all the measured proxies and five sediment Zones were identified (Figure 9). Zone I goes from 95.5 cm to 87, Zone II goes from 87 to 78.5 cm, Zone III goes from 78.5 to 58.0 cm, Zone IV goes from 58.0 to 33.5 cm and Zone V goes from 33.5 cm to 0.0 cm. The Zones detected with the CONISS, matched with the stratigraphic description of the core.

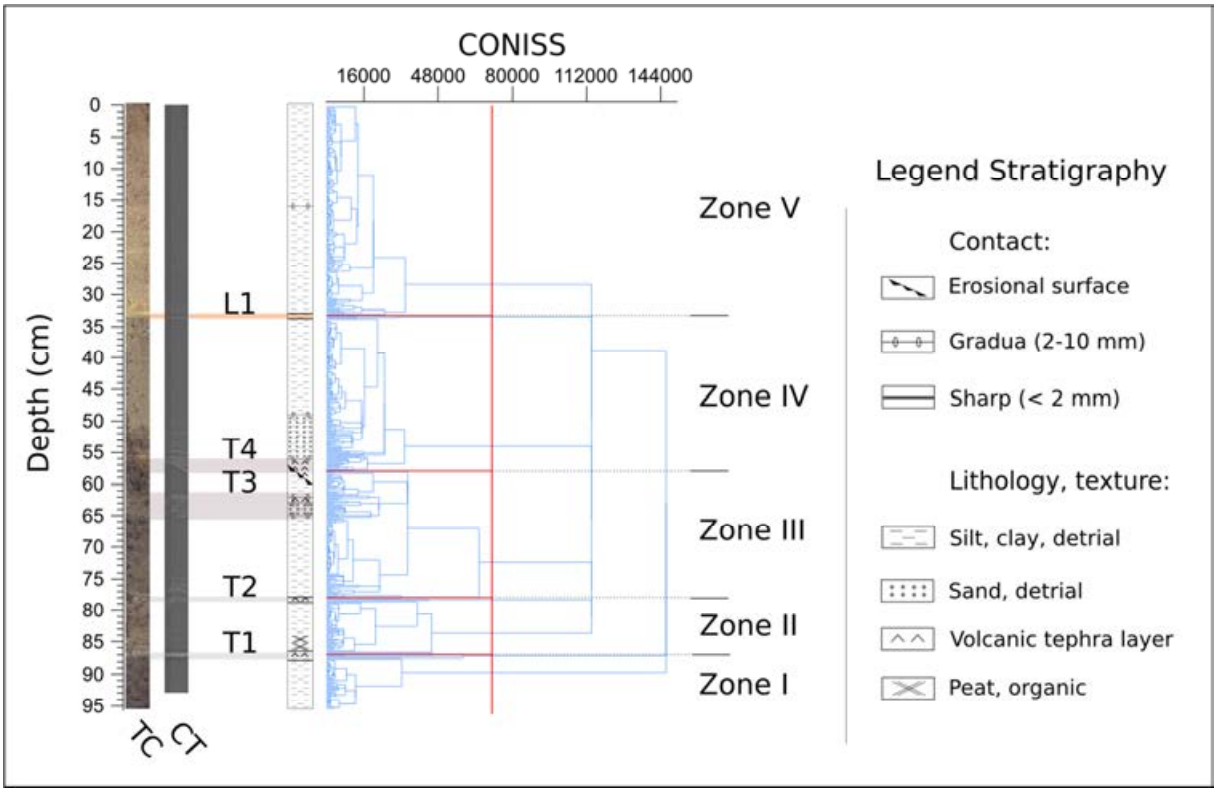

Figure 9: From left to right: true colour (TC) image; computed tomography (CT) image; stratigraphic description of the sediment core; cluster analysis (constrained incremental sum-of-squares: CONISS) to define the Zones along the sediment and legend of the stratigraphic description.

The colour of the sediment in Zone I is black (N/4.5/0), which could be related with redox conditions and higher organic matter inputs. In Zone II there are two tephras that are very similar in colour and composition. The contact of these two layers with the sediment is sharp and the colour is grey (N/4/0). The tephra layer 1 (T1) is situated from 87.2 to 86.8 cm and in its upper part it is possible to observe a peat layer until 84.3 cm. The tephra layer 2 (T2) goes from 78.9 to 78.2 cm as is seen in the true colour (TC) image. The CT image reveals that T2 reaches the 74.5 cm, which shows the real influence of T2 because its captures the whole volume of the sediment core. The colour of the rest of the Zone is black (10Y/2/1). The Zone III has a black (N/1.5/0) colour. Between 65.0 and 62.0 cm there is T3 that it can be observed clearly in the CT image and is characterized by its coarse texture. The contact Zones are gradual in the lower and upper part of the T3. Zone IV has a black (N/1.5/0) colour, which could be related with an increase of mineralogical inputs to the lake. T4 layer is in this Zone and its contact in the lower part is diagonal and erosional. The left and right sides begin at 57.3 cm and 60.2 cm, respectively, and both finish at 56.1 cm. T4 also has a granular texture. The TC and the CT image show laminations in the upper part of the T4, which are approximated 0.2 cm thick and alternate between darker and lighter layers. The laminations continue until 49.3 cm, associated with secondary tephra deposits in the sediment. Finally, Zone V is separated from Zone IV by a layer (L1). The contact of L1 is sharp and its colour is dark greyish yellow (2.5Y/4/2) and the texture of L1 is soft and thin. The upper part of L1 is dark olive brown (2.5Y/3/3) until 16 cm. From 16 to 0 cm the colour is olive black (5Y/2/2).

4.1.1. Age model

^{210}Pb age-model.

Figure 10.a shows the $^{210}Pb_t$ (blue line) at the $^{210}Pb_s$ (pink line) profiles. The $^{210}Pb_t$ activity (Figure 10.a) does not reach equilibrium at 19.5 cm, which is the deepest sample measured. The activity of $^{210}Pb_u$ is very low (11.3 ± 2 Bq cm^{-2}), which makes it very close to the $^{210}Pb_s$ (9.5 ± 2 Bq cm^{-2}). For this reason, no more samples were measured and a logarithmic fit was used to extrapolate the ages until 34 cm. The activity of ^{137}Cs is very low with an average of 8 Bq cm^{-2} (Figure 10.a) and the 1965 maximum fallout peak is not visible along the ^{137}Cs profile (Figure 10.a), probably because of diffusion along the sediment column. The ^{210}Pb ages, calculated with the CRS model (Figure 10.b), indicate that the first 19.5 cm are 92 years old.

The settlement process started in 1882 and finish in 1892 (Otero 2006), then the theoretical reach of background was set at this date to constrain the CRS model (Figure 10.b). The mass accumulation rate (MAR) calculated with the CRS model varies between 0.02 and 0.05 g cm^{-2} yr^{-1} (Figure 10.b). This indicates changes in the sedimentation rates during this period.

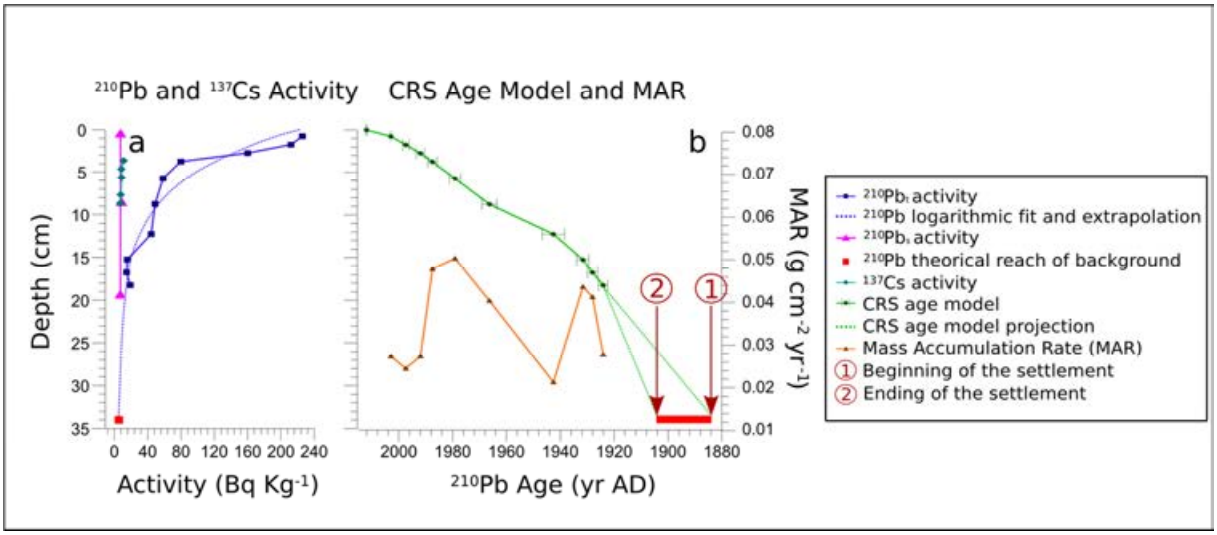

Figure 10: ^{210}Pb model. (a) $^{210}Pb_t$ activity profile. (b) Constant rate supply (CRS) model with the mass accumulation rate (MAR)

Age-depth model

The age-depth model reveals a maximum age at the bottom of the sediment of 1790 ± 150 BP. This model was constructed using the CRS ages for the first 20 cm, constrained by the age of the historical settlement at 1882 ± 10 AD. Downcore the age-depth model was constructed using the terrestrial macrofossil ages from Esp 3 and Esp 4 (Table 2). The tephra layers were eliminated from the model assuming that they were deposited in the sediment during a short period of time (Figure 11). The final age-depth model shoed in Figure 11 shows changes in the sedimentation rates are very evident. The interval between 0 and 34 cm (-62 and 101 BP) has an average sedimentation rate of 0.35 cm yr^{-1}. The sedimentation rate between 34 and 63 cm (100 and 1470 BP) is 0.017 cm yr^{-1}. Between 63 and 95.5 cm (1470 and 1790 BP) the sedimentation rate is 0.079 cm yr^{-1} (Figure 11).

Table 2: ^{14}C dates of Laguna Espejo core (LE13-2)

Sample label	Depth (cm)	Material	^{14}C yr BP	Max-min age cal. BP	Lab code
Esp 1	33.5-34.5	Bulk Sediment	2229±20	2148-2310	BE1831.1.1
Esp 2	44-45	Bulk Sediment	2174±20	2043-2158	BE1834.1.1
Esp 3	64-65	Bulk Sediment	1720±20	1535-1612	BE1837.1.1
Esp 3 leaf	64-65	Macrofosil (leaf)	1606±35	1374-1532	BE1843.1.1
Esp 4	93.5-94.5	Bulk Sediment	1899±20	1728-1836	BE1840.1.1
Esp 4.1 leaf	93.5-94.5	Macrofosil (leaf)	1908±46	1706-1908	BE1844.1.1
Esp 4.2 leaf	93.5-94.5	Macrofosil (leaf)	1837±23	1697-1752	BE1845.1.1

The ^{14}C samples, Esp 1 and Esp 2 (Table 2), where removed from the model because they had age reversal. The inversion of the bulk sediment was probably caused by the reservoir effect. As the reservoir effect was not constant through time, these ages could not be corrected with the macrofossils ages.

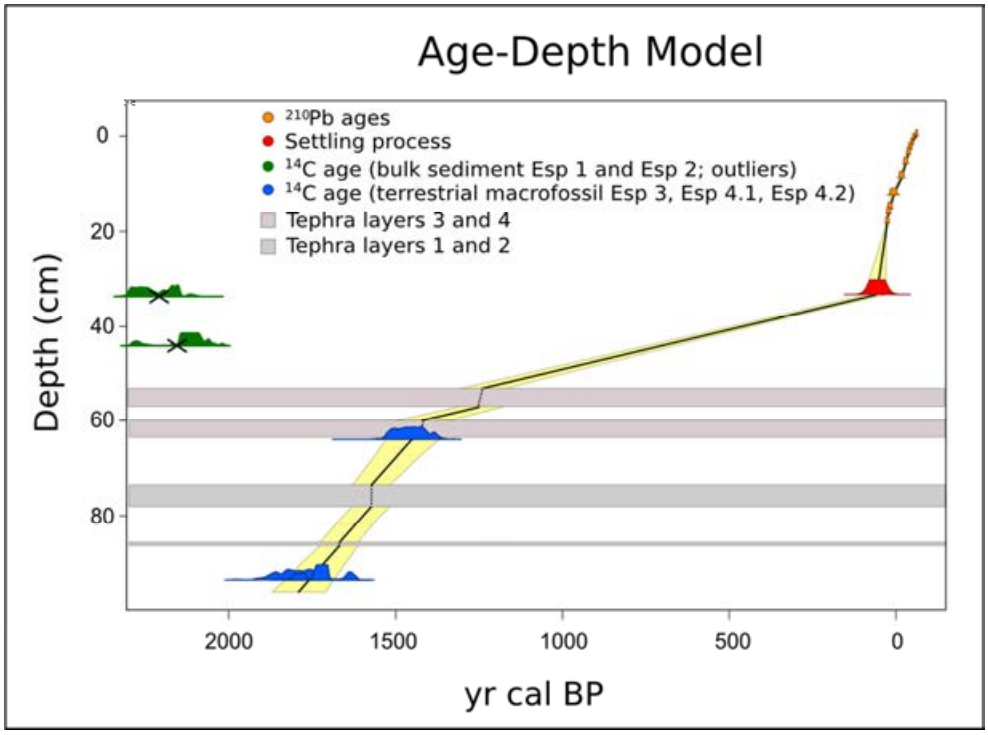

Figure 11: Age-depth model including ^{210}Pb ages, historical age and ^{14}C calibrated ages

4.1.2. Physical and biogeochemical sediment analyses

Physical sediment properties

Zone I: The water content decreases from 80 to 76 % at 91 and 92 cm, whereas the dry density and the γ-bulk density increase from 0.2 to 0.24 g cm^{-3} and from 1.08 to 1.12 g cm^{-3}, respectively. The MS

is influences by T1 and increases during this period from 40 until 340 *10^{-4} SI at T1. The mean grain size is 6 phi and the highest frequency is between 8 and 5 phi in this Zone (Figure 12).

Zone II: The water content varies from 74 to 68 %. In the tephra layers, the water content decreases down to 48 % at T1 and 32 % at T2. The dry density and the γ-bulk density are in the same range as in Zone I. In the tephra layers both densities increase. At T1 the dry density increases up to 0.6 g cm^{-3} and to 1 g cm^{-3} at T2. The γ-bulk density increases to 1.6 g cm^{-3} at T1 and until 1.4 g cm^{-3} at T2. There is a second peak of the γ-bulk density at 74 cm. In the tephra layers the MS has peaks of 300 and 340 *10^{-4} SI for T1 and T2, respectively. The mean grain size in T1 and T2 increases to 5 phi and the frequency at this point increases to 32 % (Figure 12).

Zone III: The sediment properties are stable in this Zone and similar to Zone I and II, except for T3. In this tephra layer the water content and dry density is 60 % and 0.4 g cm^{-3}, respectively. For the γ-bulk density there are two peaks at 65 and 61 cm, which are 1.28 and 1.48 g cm^{-3}, respectively. The MS peak reaches 280 *10^{-4} SI. The mean grain size is 1 phi and the highest frequency is between 3 and -1 phi (Figure 12).

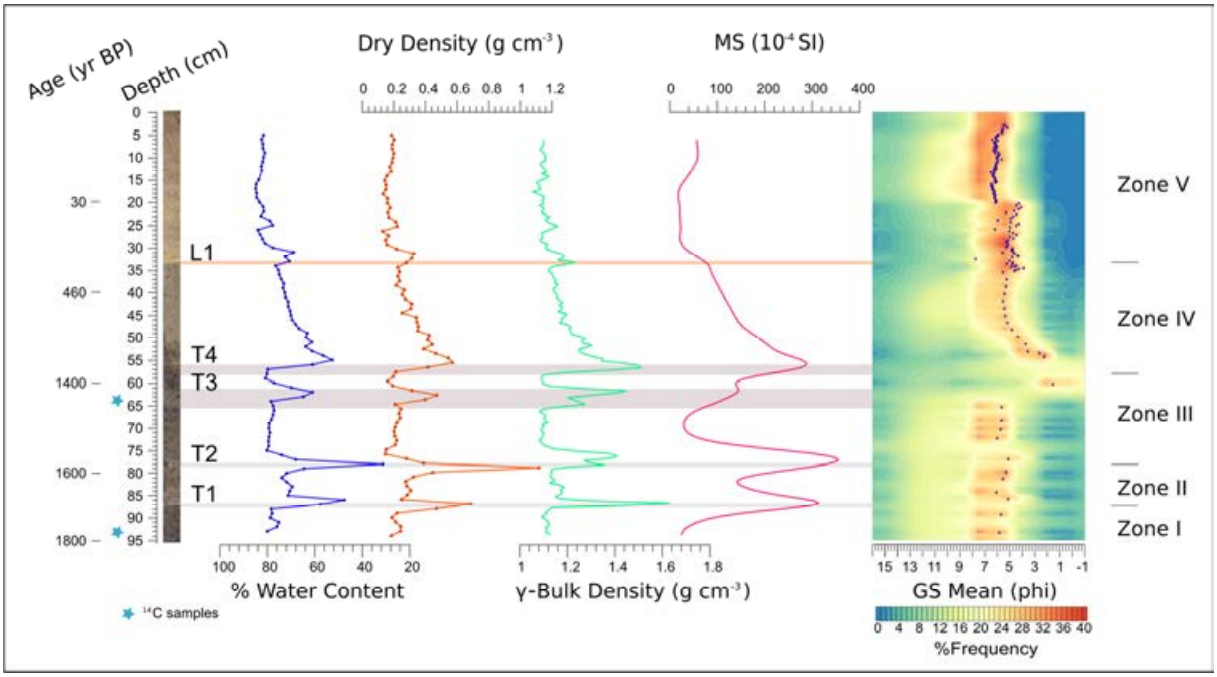

Figure 12: Sediment properties. From left to right: Percentage of water content, dry density, γ-bulk density, magnetic susceptibility (MS) and mean grain size, and grain size frequency.

Zone IV: At T4, there are high values of water content (52 %), dry density (0.58 g cm^{-3}), γ-bulk density (1.58 g cm^{-3}), and MS (280 *10^{-4} SI). Up core, there is an increase of water content and a reduction of dry density, γ-bulk density, MS and grain size until the 34 cm. This is due to the tephra layer still influencing the sediment column in Zone IV (Figure 12).

Zone V: At L1 water content decreases to 68 %, γ-bulk density, and MS increase to 1.24 g cm^{-3}, and 80 *10^{-4} SI, respectively, and the mean grain size decreases to 8 phi (Figure 12) . The frequency of grain size remains constant. At 30 and 24 cm, there are peaks in the water content, dry density and γ-bulk density. The grain size mean is different between 33 and 20 cm and between 20 and 0.0 cm. In the first part, the mean grain size ranges between 5 and 4 phi. There are two peaks of 6 phi at 24 and 23 cm. The highest frequency in this part is from 7 to 4 phi. The mean grain size in the second part is stable around 6 phi. Finally the highest frequency varies from 8 to 5 phi (Figure 12).

Organic sediment properties

Total nitrogen, total organic carbon, C/N ratio, and biogenic silica

***Zone I*:** At 93 cm there are peaks in TN and TOC. These peaks reach 1.2 % and 19 %, respectively. The C/N ratio is constant in this Zone with a value around 16 (Figure 13).

Zone II: TN and TOC are constant in this Zone, but lower than in Zone I. The values are around 0.6 % and 10 %. The C/N ratio is slightly lower than in Zone I. The value for C/N ratio is around 15. The tephra layers were not analyzed for these three variables (Figure 13).

Zone III: TN decreases from 1.2 % to 0.8 %. TOC follows the same tendency as TN, decreasing from 16 % to 14 %. However, the C/N ratio increases from 15 to 19. This means that the input of organic matter is more terrigenous in the upper part of Zone III (Figure 13).

Zone IV: TN and TOC increase until 40 cm. TN increases from 0.4 % to 0.6 % and TOC from 6 % to 8 %. From 40 cm to 33.5 cm, both variables stay constant, except at 39 cm. At this point both variables decrease slightly. The C/N ratio stays constant in this Zone, with a value around 17.5 (Figure 13).

Zone V: TN, TOC, and C/N ratio decrease at L1. The values at L1 of TN, TOC and C/N ratio are 0.2 %, 2 % and 13 %, respectively. The decrease in TN and TOC means that the major sediment input for L1 was clastic sources and the decrease in C/N ratio means that the organic matter produced at L1, was from autochthonous source (Figure 13).

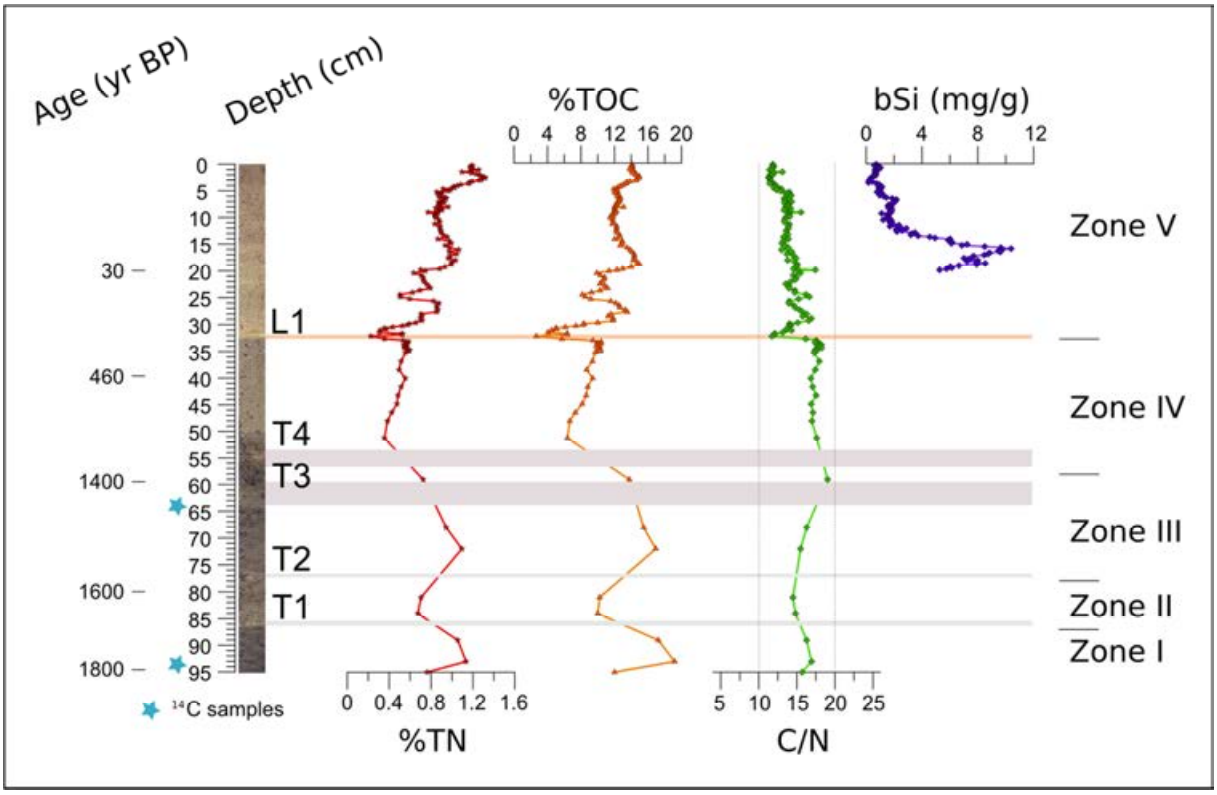

Figure 13: Organic sediment properties. From left to right: percentage of TN, percentage of TOC, C/N ratio, and bSi.

RABD$_{660;670}$ (chlorins)

Zone I: The values of RABD$_{660;670}$ are constant and oscillate between 1.04 and 1.06 (Figure 14).

Zone II: The RABD$_{660;670}$ decreases to 1.02 and 1.03 at the tephra layers T1 and T2, respectively. Between the tephra layers the RABD$_{660;670}$ values are constant around 1.04 (Figure 14).

Zone III: The RABD$_{660;670}$ increases from 1.04 to 1.08 between 77 and 65 cm. Then, the RABD$_{660;670}$ decreases to 1.02 at T3. After T3 the RABD$_{660;670}$ increases to 1.03 (Figure 14).

Zone IV: The RABD$_{660;670}$ decreases to 1.01 in T4. After T3 the values of RABD$_{660;670}$ are constant around 1.02 along Zone IV (Figure 14).

Zone V: In general, this Zone is the one with the highest RABD$_{660;670}$ values. The RABD$_{660;670}$ increases in three occasions along Zone V. The first peak is between 30 and 27 cm, where the RABD$_{660;670}$ values reach 1.09. The second peak, is at 16 cm and is the highest peak of the entire core. The third period of increase is above 5 cm, where the values are around 1.07 (Figure 14). These events are associated with an increase of the productivity in the lake, which is confirmed by the lower C/N ratio during these periods (Figure 13).

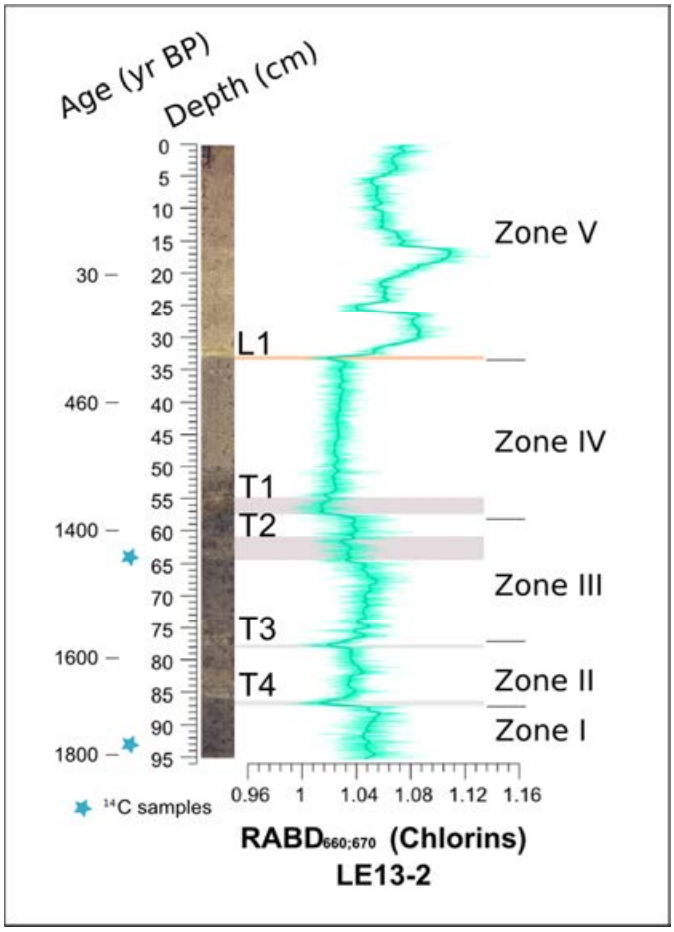

Figure 14: Chlorin content for the cores LE13-2 and LE13-3 from Laguna Espejo.

Geochemical sediment properties

Zone I: The correlation matrix for Zone I (Table 3), shows a strong correlation among the elements that come from volcanic tephra (Si, Ti, Fe, Mn, K, Sr and Ca). K and Fe are also correlated with Zr. This means that Si, Mn, and Fe are mainly related to allochthonous sources. In the case of Si and Mn, these are controlled by volcanic tephra, while Fe is controlled by both volcanic and erosive processes. The peak at 93 cm for Ti, K, Fe, Si, Sr and Ca (Figure 15) can be associated to volcanic input. Zr is higher between 95 and 89 cm. The increase of Zr can be associated with a mixture of volcanic and erosive processes in the lake.

Zone II: This Zone is highly influenced by the volcanic tephra layers. Only the elements related to volcanic sediments have a high positive correlation among them in Zone II ($R > 0.95$; Table 3). A peak of these elements (Ti, K, Fe, Si, Sr and Ca) can be seen in Figure 15 at T1 and T2. Br is highly negatively correlated with the elements associated with volcanic tephra (Table 3) and decreases (Figure 15) together with the TOC (Figure 13). Zr and Rb do not show variations with the tephra layers nor significant correlations.

Zone III: As well as in Zone II, Zone III is highly influenced by tephra layers. There is a high positive correlation amongst the elements related to volcanic tephra (Table 3). Figure 15 shows a peak at T3 for these elements. Between 69 and 65 cm there is an increase in Zr, Rb, Sr and K (Figure 15) that

could be associated to soil erosion because they are significant (p-value < 0.05) positively correlated (0.2< R <0.39; Table 3). As well as in Zone II, there is a negative correlation between Br and K, Ca, Ti, Mn, Fe, and Sr (Table 3) and Br also increases and decreases accordingly with TOC (Figure 13).

Zone IV: This Zone is influenced by volcanic tephra (T4) and soil input. Figure 15 shows a peak of the elements related to volcanic sediments at T4. As in the previous Zones, there is a high level of correlation between the elements associated with volcanic tephra (Table 3). Br increases at T4 (Figure 15), probably because there is a mixture between organic matter and minerogenic material. As T4 has a coarse grain size, the organic material could percolate. Ti, K, Fe, Si, and Zr increase between 52 and 44 cm (Figure 15). The correlation matrix for this Zone indicates a significant positive correlation of Zr with Ti, K, Fe and Si (Table 3). Between 52 and 44 cm there is an increase of Rb (Figure 15).

Zone V: This Zone was divided in Zone V.1 (between 33 and 15 cm) and Zone V.2 (between 15 and 0 cm) because there is a clear change in the sediment composition at 15 cm:

> *Zone V.1:* There is a peak of Ti, K, Fe, Si, Sr, Rb, and Zr at L1, 25 cm, and 23 cm (Figure 15). The peaks are associated with soil erosion events because they are highly correlated with Zr (Table 3 cont.). Br (Figure 15) follows the TOC curve (Figure 13) and is anticorrelated with the elements related to volcanic tephra and soil along Zone V.1 (Table 3 cont.).
>
> *Zone V.2:* The Si is highly correlated with K and with Ca. This means that Si in the sediment is controlled by both, allochthonous and autochthonous input. Ca is highly correlated with Ti and Sr, which indicates that Ca input could derived from both allochthonous and autochthonous sources. Finally, Fe is highly correlated with Ti, which means that Fe is controlled by detrital input (Table 3 cont.). Zr does not have any significant correlation in this Zone, which suggests that the origin of the elements is autochthonous.

Table 3: Correlation matrices (R values) for Laguna Espejo by Zone

Zone		K	Ca	Ti	Mn	Fe	Br	Rb	Sr	Zr
I	Si	0.33	**0.59**	**0.83**	0.15	**0.55**	-0.10	0.07	0.11	0.28
	K		**0.76**	0.44	**0.67**	**0.72**	0.01	0.15	**0.73**	**0.59**
	Ca			**0.64**	**0.65**	**0.79**	-0.10	0.15	**0.65**	0.38
	Ti				0.37	**0.71**	-0.24	0.01	0.17	0.21
	Mn					**0.66**	0.08	0.07	**0.63**	0.43
	Fe						-0.18	-0.06	**0.54**	**0.50**
	Br							0.07	0.18	0.25
	Rb								0.24	0.12
	Sr									0.50
II	Si	**0.99**	**0.99**	**0.98**	**0.95**	**0.96**	**-0.69**	0.11	**0.89**	-0.10
	K		**0.99**	**0.99**	**0.95**	**0.97**	**-0.73**	0.10	**0.91**	-0.09
	Ca			**0.99**	**0.96**	**0.98**	**-0.73**	0.11	**0.92**	-0.09
	Ti				**0.95**	**0.97**	**-0.75**	0.10	**0.91**	-0.09
	Mn					**0.98**	**-0.71**	0.15	**0.95**	-0.15
	Fe						**-0.74**	0.16	**0.97**	-0.13
	Br							-0.24	**-0.71**	0.11
	Rb								0.16	0.16
	Sr									-0.11
III	Si	**0.59**	**0.62**	**0.72**	**0.52**	**0.61**	-0.31	-0.15	0.39	0.14
	K		**0.73**	**0.74**	**0.66**	**0.74**	**-0.56**	0.14	**0.72**	0.39
	Ca			**0.86**	**0.82**	**0.92**	**-0.62**	0.03	**0.86**	0.23
	Ti				**0.76**	**0.92**	**-0.68**	-0.05	**0.76**	0.21
	Mn					**0.86**	**-0.63**	0.11	**0.81**	0.24
	Fe						**-0.74**	0.05	**0.91**	0.29
	Br							-0.14	**-0.69**	-0.19
	Rb								0.09	0.14
	Sr									0.28
IV	Si	**0.87**	**0.51**	**0.92**	0.39	**0.81**	-0.21	0.02	0.44	0.42
	K		**0.76**	**0.81**	**0.64**	**0.91**	-0.36	0.10	**0.70**	0.36
	Ca			0.44	**0.79**	**0.79**	-0.47	0.14	**0.86**	0.04
	Ti				0.33	**0.81**	-0.22	0.04	0.38	0.43
	Mn					**0.67**	**-0.52**	0.10	**0.75**	0.14
	Fe						-0.42	0.11	**0.79**	0.38
	Br							-0.11	-0.49	0.09
	Rb								0.17	-0.05
	Sr									0.14

Bold blue/red: strong positive/negative correlation ($R \geq 0.5$ / $R \leq -0.5$).

Normal blue/red: positive/negative correlation ($0.5 \geq R \geq 0$ / $0 \leq R \leq -0.5$).

Green background: significant correlation (p-value ≤ 0.05).

Table 3 (Continued)

Zone		K	Ca	Ti	Mn	Fe	Br	Rb	Sr	Zr
V.1	Si	**0.83**	**0.84**	**0.82**	0.49	**0.88**	-0.38	0.33	**0.78**	**0.73**
	K		**0.90**	0.48	**0.58**	**0.71**	-0.36	0.44	**0.75**	**0.67**
	Ca			**0.62**	**0.65**	**0.85**	-0.36	0.43	**0.89**	**0.73**
	Ti				0.23	**0.91**	-0.39	0.17	**0.67**	**0.67**
	Mn					0.47	-0.24	0.21	**0.57**	0.36
	Fe						-0.44	0.31	**0.84**	**0.80**
	Br							-0.19	-0.30	-0.32
	Rb								0.37	0.37
	Sr									**0.72**
V.2	Si	**0.69**	**0.92**	0.46	**0.62**	-0.04	-0.02	-0.05	**0.70**	0.05
	K		**0.82**	**0.78**	**0.64**	0.45	-0.20	-0.04	0.45	0.17
	Ca			**0.65**	**0.74**	0.18	-0.13	-0.12	**0.70**	0.09
	Ti				**0.55**	**0.82**	-0.19	-0.05	0.39	0.19
	Mn					0.26	-0.12	0.02	**0.52**	-0.05
	Fe						-0.20	0.05	0.04	0.16
	Br							-0.16	-0.06	0.01
	Rb								-0.04	0.09
	Sr									0.16

Bold blue/red: strong positive/negative correlation ($R \geq 0.5$ / $R \leq -0.5$).

Normal blue/red: positive/negative correlation ($0.5 \geq R \geq 0$ / $0 \leq R \leq -0.5$).

Green background: significant correlation (p-value ≤ 0.05).

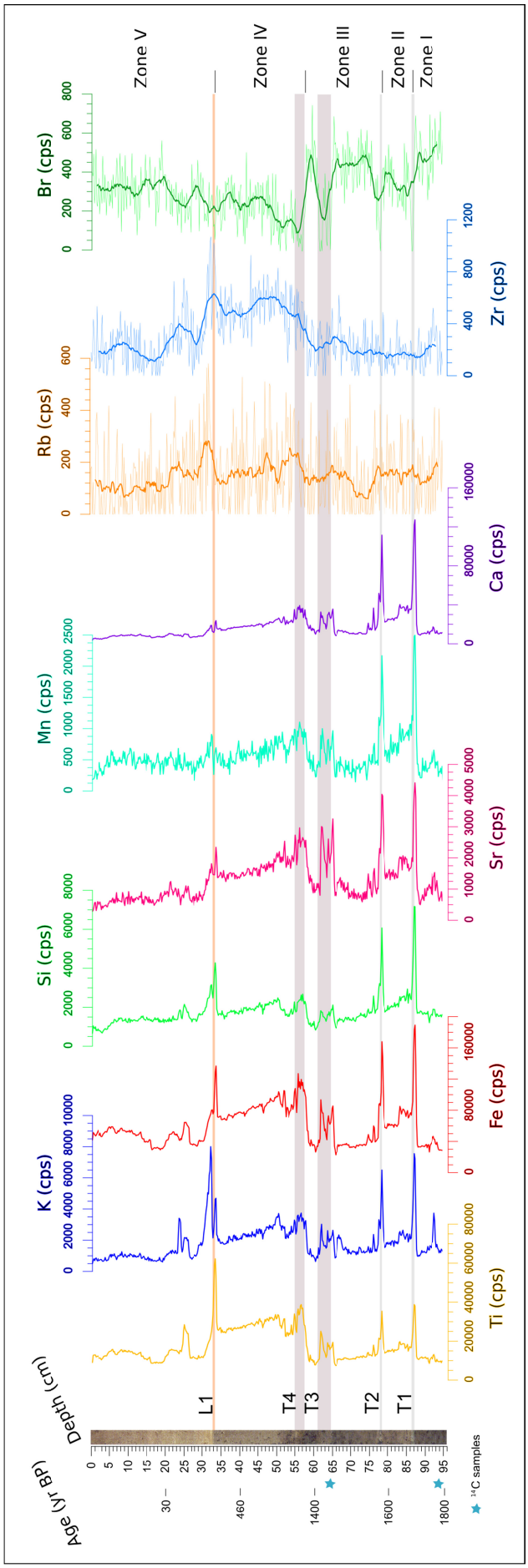

Figure 15: Selected XRF elements. Ti, K, Fe, Si and Sr are associated with terrigenous inputs and with volcanic tephra composition. Ca is more associated with volcanic tephra inputs. Rb and Zr are associated with terrigenous inputs, and Br is associated with organic matter.

4.1.3. Statistical ordination and classification.

The k-mean clustering on the biogeochemical proxies reveals four significant clusters (Figure 16). The PCA had two significant PCs, explaining 50 % of the variance together. PC1 explains 35 % of the variance and is related to inorganic proxies. The origin of these elements can be terrigenous or volcanic (Ca, Mn, Si, Sr, K, Fe, Rb, Ti, and Zr). PC2 explains 15 % of the variance and is related to organic proxies. The organic proxies are bSi, TOC, Br, TN and $RABD_{660;670}$ (chlorins).

Figure 16 shows the PCA biplot. Different colours indicate the three different clusters from the k-means. Clusters 1 and 2 are related to organic and inorganic sedimentation, respectively. Clusters 3 and 4 are related to volcanic tephra and soil layers. Cluster 3 corresponds to T4 and L1, and cluster 4 corresponds to T1 and T2, which indicates that T1 and T2 are richer in Ca, Mn and Si than T3 and T4.

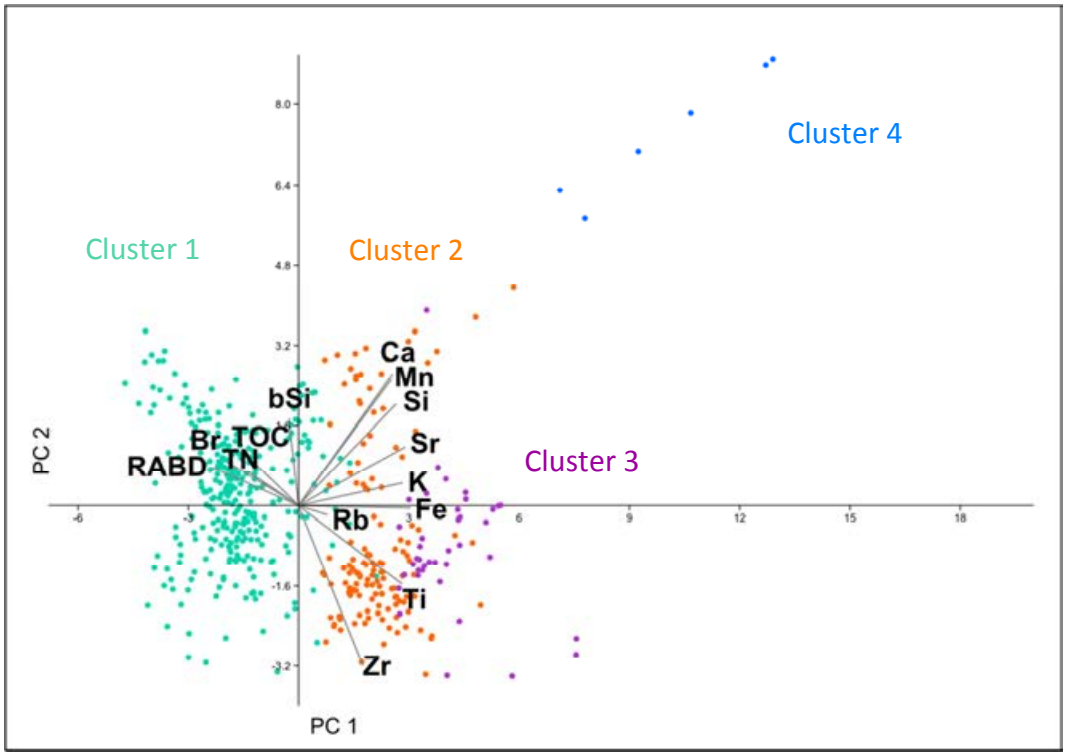

Figure 16: K-means cluster analysis (cluster 1: green, cluster 2: orange, cluster 3: green, and cluster 4: blue) plotted against the PCA. PC1: 35 % explained variance; PC2: 15 % explained variance.

4.2. Calibration-in-time

Temperature and precipitation.

The temperature and precipitation records were obtained from the CRU 3.21TS reanalysis data between 1940 and 2009. The temperature data from Laguna Espejo is significant and highly positively correlated with southern South America from 30 °S (Figure 17.a). The correlation is also significant inside the dashed lines where the p-values are smaller than 0.05 (Figure 17.a). On the other hand, the precipitation data from Laguna Espejo are significantly positively correlated between 35 °S and 45 °S of southern South America (Figure 17.b).

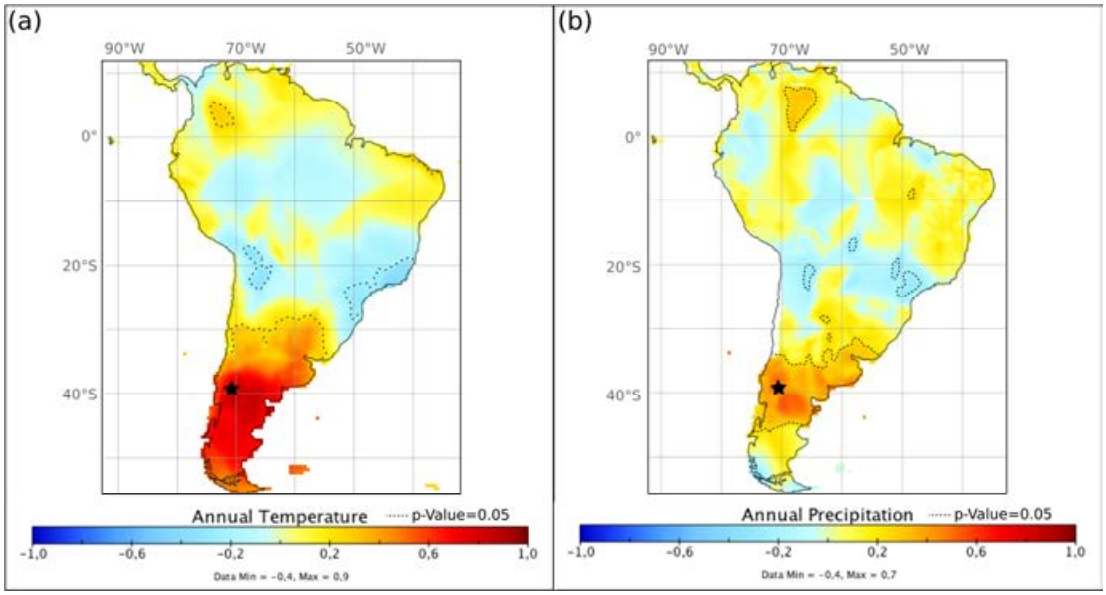

Figure 17: (a) Annual temperature correlation map. (b) Annual precipitation correlation map. In both maps the correlation is significant in the areas surrounded by the dashed line where the p-values are smaller than 0.05.

Table 4 shows the correlation coefficient (R; p-value < 0.05) adjusted for autocorrelation (p_{corr} < 0.05) between each proxy and monthly temperature record from 1940 to 2009. Mn has a high significant (p-value < 0.05; p_{corr} < 0.05) correlation with September–October temperatures. TOC, bSi, Fe, Ti and MAR have a high significant (p-value < 0.05) correlation but p_{corr} > 0.05, which means that is not significant for autocorrelation. Chlorin, density and grain size did not have any significant correlation.

Table 4: Correlation of monthly temperature with each proxy.

Proxy	Period	R	p-value	p_{corr}
Chlorin	NC	NC	NC	NC
TOC	September	0.58	0.020	0.197
bSi	June	0.51	0.008	0.161
Br	October - December	-0.47	0.049	0.185
Mn	September - October	-0.61	0.000	0.013
Ca	September - October	-0.46	0.025	0.996
Sr	August - November	-0.47	0.001	0.075
Fe	June	-0.63	0.001	0.102
Zr	July - August	0.38	0.047	0.953
Ti	June	-0.53	0.007	0.181
Rb	April - May	0.46	0.047	0.607
MAR	September	0.67	0.001	0.073
Density	NC	NC	NC	NC
Grain size mean	NC	NC	NC	NC
K	October	-0.54	0.003	0.069

R = correlation coefficient; p-value < 0.05 = significant; p_{corr} < 0.05 = significant for autocorrelation; NC = no significant correlation

Table 5 shows the correlation coefficient (R; p-value < 0.05) adjusted for autocorrelation (p_{corr} < 0.05) between each proxy and monthly precipitation record from 1940 to 2009. Chlorin has a high significant (p-value < 0.05; p_{corr} < 0.05) negative correlation with April (-1)–February precipitation (Table 5). The higher significant correlations were found for: chlorin, Ca, Fe, Ti, grain size mean, and K, but they were not significant for autocorrelation. Br, Sr, and MAR did not show any significant correlation.

Table 5: Correlation of monthly precipitation with each proxy.

Proxy	Period	R	p-value	p_{corr}
Chlorin	April (-1) - February	-0.76	0.049	0.008
TOC	April - June	-0.43	0.042	0.751
bSi	February	0.46	0.018	0.999
Br	NC	NC	NC	NC
Mn	June	-0.39	0.038	0.934
Ca	August	0.59	0.003	0.436
Sr	NC	NC	NC	NC
Fe	February	-0.54	0.008	0.990
Zr	February	0.30	0.020	0.999
Ti	February	-0.62	0.001	0.182
Rb	May - July	-0.41	0.035	0.506
MAR	NC	NC	NC	NC
Density	June - July	0.40	0.027	0.463
Grain size mean	June (-1) - January	0.50	0.040	0.624
K	April - September	0.57	0.048	0.189

R = correlation coefficient; p-value < 0.05 = significant; p_{corr} < 0.05 = significant for autocorrelation; NC = no significant correlation; month (-1) = month year before.

The PCA from the period between 1940 and 2009 AD has just one significant PC that explains the 55 % of the variance (Figure 18). The organic proxies TOC, TN, and $RABD_{660;670}$ are negatively correlated with PC1 and the inorganic proxies Fe Ti, K, Mn, Sr, and Ca are positively correlated with PC1 (Figure 18).

Two groups are clearly identified in the biplot in Figure 18. The first group is associated with the organic proxies and corresponds to the period between 1985 and 2009. The second group is associated with the inorganic proxies and corresponds to the period between 1940 and 1984 (Figure 18). The explanation for this would be that, between 1940 and 1984, the sediment signal is dominated by inorganic inputs to the lake. In contrast, between 1985 and 2009, the sediment signal would be dominated by organic input which would be produced it in the lake (Figure 13).

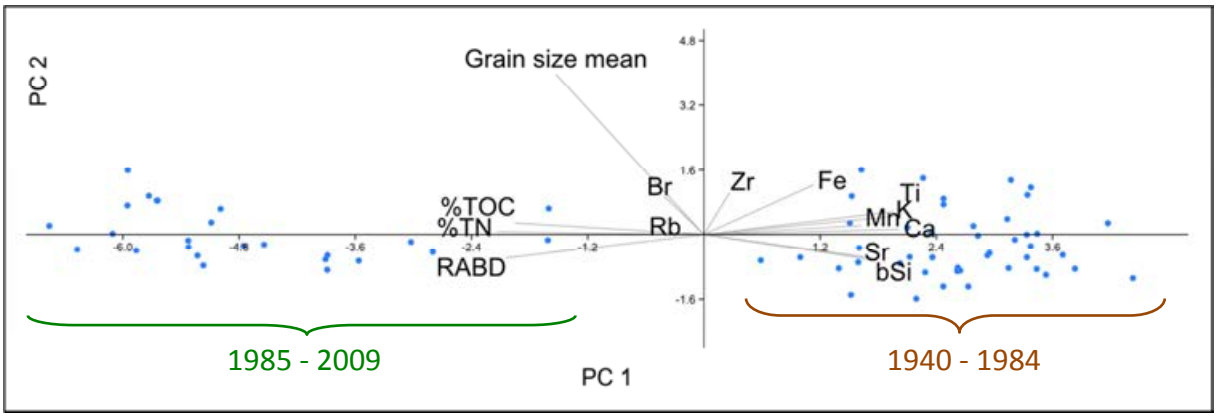

Figure 18: PCA for the calibration period (1940 to 2009). PC1 = 55 % explained variance.

In order to discard a "false significant correlation", two plots were made: one temperature (September to October) together with Mn (Figure 19.a), and the other precipitation (April (-1) to February) together with $RABD_{660;670}$ (Figure 19.b). Between 1980 and 1990 AD, there is a rapid increase of Mn and a decrease in $RABD_{660;670}$, which is not reflected by the climatic data: neither temperature (Figure 19.a) nor precipitation (Figure 19.b). This argument, along with the presence of only one significant PC in the PCA, explains why the correlations between Mn and temperature (Table 4), and $RABD_{660;670}$ and precipitation (Table 5) were considered a "false significant correlation".

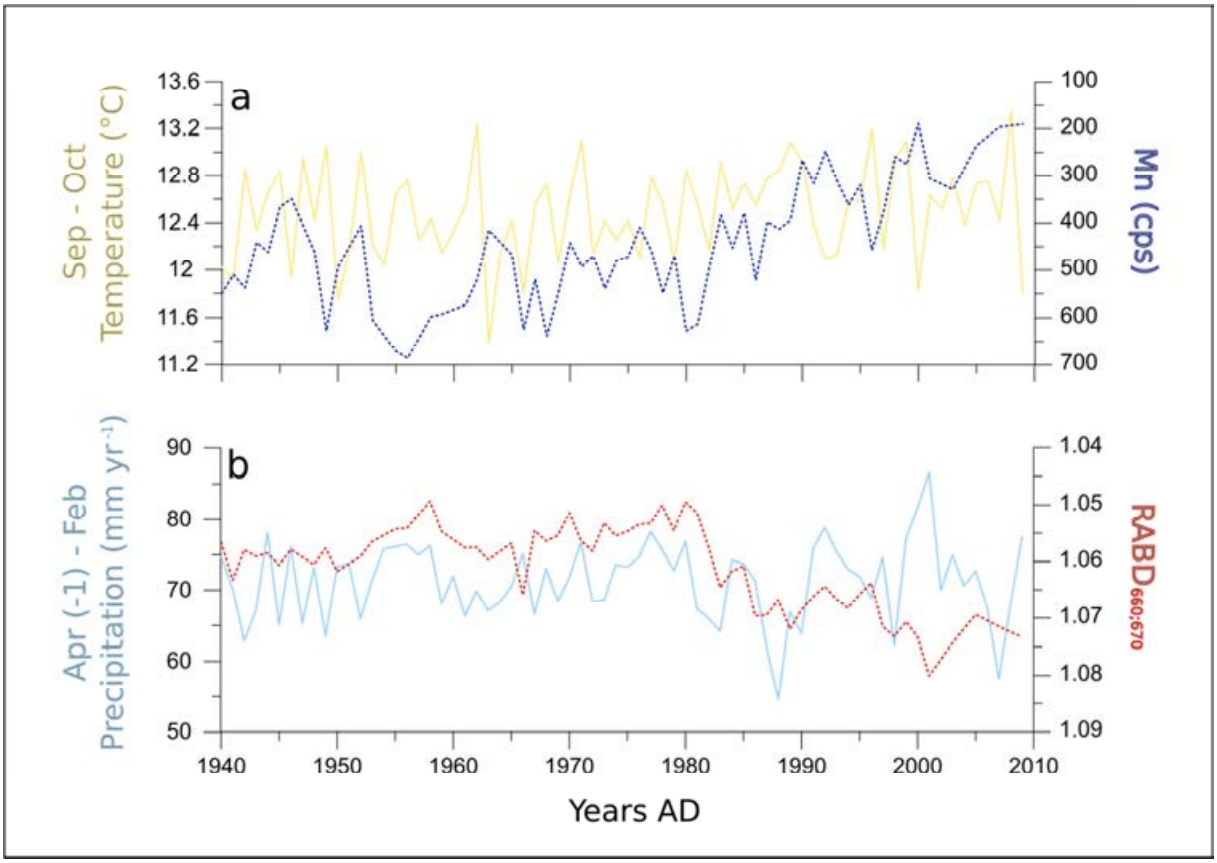

Figure 19: (a) Time-series of temperature (from September to October) versus Mn. (b) Time-series of precipitation (from April (-1) to February) versus $RABD_{660;670}$.

5. Discussion

5.1. Age-depth model

CRS model

The CRS model was constructed using ^{210}Pb ages. There is only a small amount of ^{210}Pb in lake sediments in the Southern Hemisphere. This is due to small amount of landmass in the Southern Hemisphere. As the ^{210}Pb comes from the decay of ^{222}Rn, a small amount of landmass means a smaller amount of ^{210}Pb production. Nevertheless, it was possible to detect the ^{210}Pb in the sediments of Laguna Espejo and construct the CRS model.

The CRS model assumes a constant rate supply of ^{210}Pb over time. This is not always the case: changes in year-to-year precipitation regimes, for example, lead to changes in the input of ^{210}Pb (von Gunten et al. 2009b). This is why it is necessary to constrain the model with another independent marker. The most common marker used is the peak of ^{137}Cs produced by nuclear essays in the mid-20th century (Cohen 2003). Unfortunately, it was not possible to measure this peak in the sediments of Laguna Espejo. Therefore, the historical date of European settlement between 1882 and 1892 was used to constrain the CRS model.

^{14}C ages

There are two possible explanations for the reservoir effect in the ESP 1 and ESP 2 samples. One explanation could be methane diffusion from old sediments. Methane is produced in the sediment by anaerobic decomposition of organic matter and can diffuse from deeper (older) sediments and reach the water column (Håkason and Jansson 2002). The methane would be depleted in ^{14}C, which would produce dates with older ages. In the water column, the methane is oxidized to CO_2 (Meyers and Terrance 2001). The CO_2 in the water column forms part of the dissolved inorganic carbon (DIC; Cohen 2003). The DIC is consumed by the organism that live in the water column and later deposited in the lake bottom when thy die. When these organisms die, they are deposited on the lake bottom. As the deposited organism would have depleted ^{14}C, the sediment would be dated to be older than it really is. Such a situation of methane outgassing could happen during the period that ESP 1 and ESP 2 were formed. In such a scenario, the bulk sediment of ESP 1 and ESP 2 would exhibit a considerable reservoir effect.

Another explanation for the reservoir effect in ESP 1 and ESP 2 could be volcanic activity. This has been reported in Iceland by Sveinbjörnsdóttir et al. (1992). After an eruption, CO_2 depleted in ^{14}C is expelled from volcanoes. This CO_2 is consumed by photosynthetic organisms, resulting in older ages when its organic matter is dated (Björc and Wohlfarth 2001). In Laguna Espejo, it seems unlikely that this would cause a reservoir effect; the reservoir effect would be constant through time, which is not the case of the sediments from Laguna Espejo. The age discrepancy could also be due to sediment redeposition (Cohen 2003). The redeposition process consists in old material being deposited on

young sediments. The old material could come from the basin, reaching the lake sediment through runoff or could result from erosive processes within the lake bottom (Håkason and Jansson 2002).

5.2. Volcanic activity

Laguna Espejo is located in a highly active volcanic area. Four tephra layers were identified along the core: T1, T2, T3, and T4. From these four tephras, T1 is similar to T2, and T3 is similar to T4. The similarity was found in grain size, colour and thickness. According to the age-depth model, the ages of each tephra layer are: T1 = 1700 BP, T2 = 1600 BP, T3 = 1500 BP, and T4 = 1300 BP.

The closest volcanoes to Laguna Espejo are Volcan Lonquimay, Volcan Llaima, and Volcan Villarrica, located at ~50 km distance from Laguna Espejo. Further away, Volcan Lanin is located at ~90 km, and Volcan Calbuco at ~260 km distance from Laguna Espejo, which may also influence the lake. Depending on wind direction and the height of the eruptive column, tephra can travel hundreds of kilometres. The further away the volcano, the smaller the grain size and thickness of the tephra layer (Pfeiffer et al. 2005). Based on this assumption, grain size of T1 and T2 may indicate that they come from volcanoes located further away than T3 and T4.

Considering the record published by Fontjin et al. (2014) that consist in a summary of the main eruptions reported from the CSVZ and based in the age of the tephras: T1 and T2 could come from Volcan Calbuco; T3 and T4 could come from one of several volcanoes close to Laguna Espejo. The most likely candidates for T3 and T4 are the eruptions from Volcan Lonquimay (1290±70 cal. BP), Volcan Villarrica (1480±90 cal. BP), and Volcan Lanin (1330±80 cal. BP). Although no studies exist about eruptions of Volcan Llaima during the periods of T3 and T4, it is known to be one of the most active volcanoes since 310 years BP (Fontjin et al. 2014). A geochemical analysis is needed to determine the exact source of the tephra layers. This kind of analysis is beyond the scope of this Master Thesis, but it would be considered as an outlook.

5.3. Pre-Columbian landscape alteration

An increase in Zr and Rb in Zone VI (Figure 15) provides evidence of erosion in the Laguna Espejo basin. According to the age-depth model, this erosion period occurred at 900 cal. BP (960 yrs cal. AD). The rest of the elements from the XRF, together with the organic proxies, do not undergo significant shifts during this period. This could mean that the erosion was caused by pre-Columbian human activities that could have been less intensive than the Settlers agriculture practice.

The Mapuche are the indigenous people that inhabit the Araucania between the Biobío and Imperial rivers (Figure 20) (Torrejón and Cisternas 2002). The Mapuche people evolved from a hunting and gathering society to an agriculture society between 500 and 1000 AD (Dillehay 1990). The Mapuche's agriculture production was consumed by their population. Their techniques were thought to be environmentally sustainable (Torrejón and Cisternas 2002). First, they needed to clear the dense forest in order to have fields for cultivation. To achieve this, they used a technique known as clear-cutting (Dillehay 1990; Otero 2006).

The clear-cutting technique begins with burning the forest in a controlled way. After the burning, the soil is rich in nutrients and perfect for growing crops and grass. This soil fertility does not last for a long time (depending on the climate and geographical factors it may last between 2 to 7, or more years (Dillehay 1990). After the fertility of the soil is lost, the terrain is abandoned. In summary, one clear-cut cycle would be: clear, burn, sow, harvest, fallow, and then regrowth of a new forest (Dillehay 1990). The Chilean forest could regenerate quickly, meaning that this technique was sustainable over time (Otero 2006). The possibility therefore exists that some Mapuche settlements were formed around Laguna Espejo around the year 1000 AD. Their clear-cutting activities would cause an episode of erosion, and this would be reflected in an increase of the terrigenous elements such as Zr and Rb (Figure 15).

Landscape disturbances by indigenous people is not a new concept. McWethy et al. (2010) recorded landscape alteration by the aborigines in New Zealand. The aborigines caused fires that burned about 40 % of the forest in New Zealand. In order to know if the Mapuche people influenced erosion around Laguna Espejo, it would be necessary to include more proxies such as pollen and charcoal. In addition, a study of several lakes in Araucania would give an overview of the widespread of the environmental impact of Mapuche people in this region.

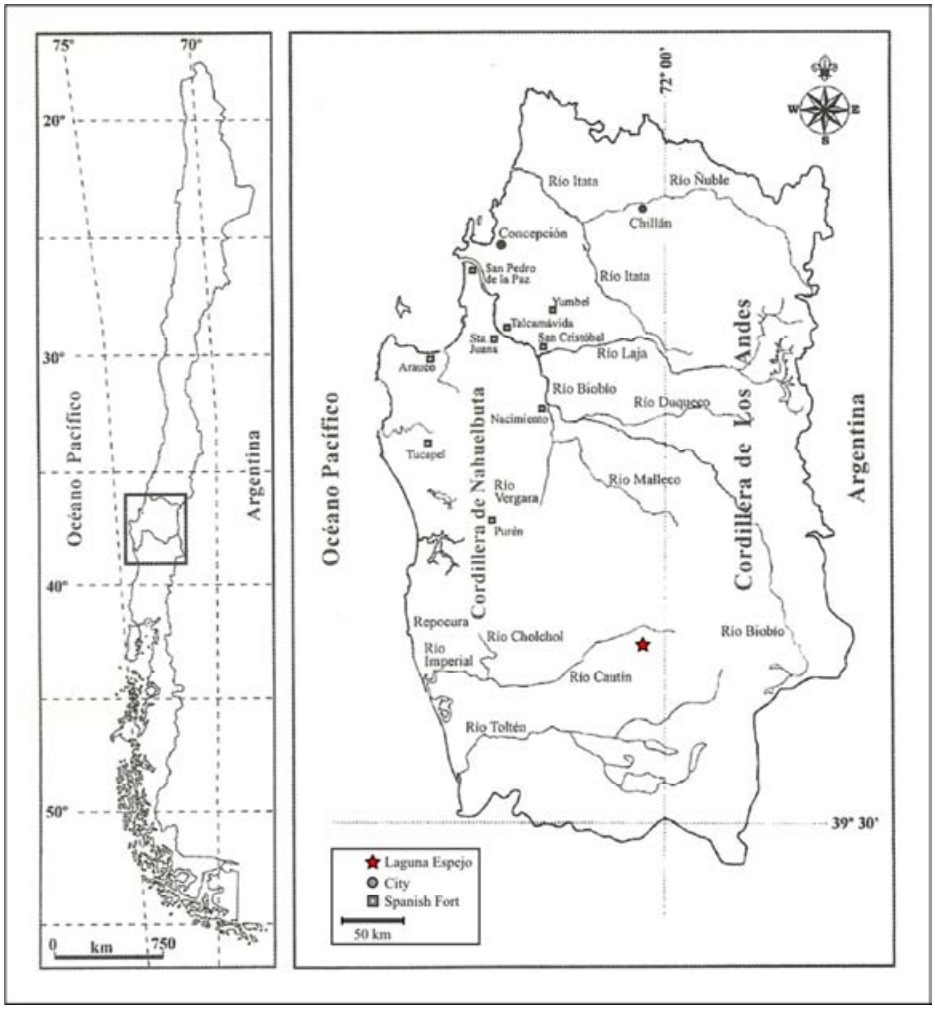

Figure 20: Historical map representing the Araucania at the end of the 17th century (modified from Torrejón and Cisternas 2002).

5.4. 19th century European settlement (1882 to 1940 AD; 33 to 13 cm sediment depth)

European settlement at the end of the 19th century caused major land-use changes in southern Chile. In 1882, the Chilean government won the war against the Mapuche in the Araucania (Otero 2006). The area between the Malleco and Toltén rivers (Figure 20) was immediately declared a settlement area in 1883 (Otero 2006). From this area, 2 million hectares were given to the new European settlers. The settlement policies increased agricultural activities without considering the sustainable use of the natural resources of the area (Otero 2006). As a result, large fires occurred in Araucania (Figure 21). Burning the forest was the mechanism used by the settlers to clear the land and convert it into grassland and cropland (Verniory 2001; Otero 2006).

Figure 21: Photograph of the forest after the fires. Loncoche, 1930 (Otero 2006)

The high variability observed in the organic proxies (TN, TOC, C/N ratio, chlorins; Figure 13), reflect the large impact of the forest clearance on Laguna Espejo after 1882. Moreover, variations in terrigenous elements, such as Ti, K, Fe, Si Rb and Zr (Figure 15), indicate also strong changes in the sediment supply.

After the fires, the vegetation cover disappeared, allowing precipitation to erode the uncovered soil. The eroded soil went directly into the lake and formed part of the lake sediments, which increased the minerogenic and nutrient content of the lake sediment (Koroluk and de Boer 2007; Smol 2001; Cohen 2003). This would explain the increase in the terrigenous elements in L1 (1882 AD) and at 25 cm depth (1910 AD). This erosion process increases the nutrients supply, which, in conjunction with fertilisers the lake and triggers primary productivity (Araneda et al. 2013). This differs from the Mapuche usage because their agriculture was probably less intensive than of the settlers. The increase in organic matter and productivity is observed at 27 cm (1910 AD) and 20 cm (1920 AD). This indicates that there were at least two episodes of forest clearance in the basin of Laguna Espejo during the settlement period.

5.5. Post-settlement (1940 to 2013 AD; 13 to 0 cm sediment depth)

In Laguna Espejo, the MAR decreases during the period from 1940 to 1980 and the proxies from both organic and inorganic origin remain constant. At this point, the lake-environment system may have been in equilibrium with the erosion processes occurring in the watershed. In addition, the forest in the basin may have started to recover. The environmental crisis provoked by the fires during the first half of the 20th century led the government to create new regulations concerning forest exploitation. The government began a process of reforestation in 1940, which attempted to stop the erosion caused by forest clearance (Otero 2006). This appears to have affected the sediments of Laguna Espejo, due to the vegetation acts as a sediment trap, thus the MAR between 1940 and 1980 was lower.

Figure 22: Evidence of human influence in Laguna Espejo, January 28th 2013 (Photography by Patricia Jana Pinninghoff).

5.6. Climate signal

The period between 1940 and 2009 AD corresponds to the interval selected for the climate calibration of Laguna Espejo. The temperature and precipitation data used was from monthly reanalysis data and was used to search for a climate signal in the sediment. The agriculture practices between 1980 and 2013 AD, in the basin of Laguna Espejo (Figure 22) increase the amount of available nutrients and led to more eutrophic conditions (Figure 13). Separating the eutrophication signal from the climatic signal in lake sediments can be challenging and statistical tools like PCA analysis are needed (Smol 2001; von Gunten et al. 2009a; Amann et al. in review).

Amann et al. (in review) were successful in splitting the climate and eutrophication signal in Lake Zabinskie, Northern Poland. They used two independent PCs, one related to climate and the other to eutrophication. This was not the case in Laguna Espejo, where the PCA had one significant PC (Figure 18) mainly influenced by proxies related to human activities and where a climate signal is not present. Figure 22 clearly shows how cattle impacts the lake shoreline, and it is likely that the cattle manure provoked eutrophication of the lake (Figure 13 and Figure 14). Similarly, McWethy et al.

(2010) found that the European settlers and the aborigines caused environmental impacts that overshadowed the climate signal in their study of lake sediments in New Zealand. Araneda et al. (2013) found that the fires caused by the European settlers generated an increase in the eutrophication of lakes in the Chilean Patagonia. In summary, the impact that the settlement process provoked in the Laguna Espejo basin, together with the intensive agriculture practices at the end of the 20th century, overshadows the climatic signal for the proxies measured in the sediments of Laguna Espejo.

6. Conclusions and Outlook

6.1. Conclusions

The aim of this Master thesis was to distinguish between the climate signal and the anthropogenic signal in Laguna Espejo (39°) and to identify possible volcanic influences. To achieve these goals, several biogeochemical analyses were performed on the sediments of Laguna Espejo. Later, the measured proxies were statistically analysed in search of a climatic component. From these analyses we can conclude the following:

Volcanic influences

The four tephra layers found in Laguna Espejo prove that volcanic eruptions influenced the sediments of Laguna Espejo. Furthermore, it was possible to identify potential sources of the tephras according to the record of historical eruptions from surrounding volcanoes.

Land-use change and climate signal

The change at 33 cm depth in the sediment core corresponds to the arrival of the European settlers after 1882 AD. This change is visible at first sight by a drastic change in the colour of the sediment core. The measured proxies also change above 33 cm. The lake sediments exhibit their highest variability between 1882 and 1940 AD. This variability is associated with the clearance of the forest in the Laguna Espejo basin. After 1940 AD, the government began reforestation measures for soil and water conservation, which helped to reduce the erosive process into the lake. Elements that come from soil erosion as well as the organic proxies do not change during this period. TOC and TN increase between 1985 and the present. This increase is associated with more eutrophic conditions in the lake. The eutrophic conditions appear to be caused by an increase of nutrient inputs to the lake due to agriculture practices in the lake basin.

The chosen calibration period for identifying a climate signal was between 1940 and 2009. The PCA used to distinguish the climate signal from the anthropogenic signal had just one significant PC related to eutrophication. Thus, the dominant signal in the lake sediments of Laguna Espejo is the anthropogenic impact and not the climate signal. This is why the multi-correlation analysis used to compare the proxies with climate data was not successful. Thus it is possible to conclude that the 20^{th} century changes in Laguna Espejo caused by European settlers overshadow the climate signal in the lake.

6.2. Outlook

The age reversal in the climate model of ESP 1 and ESP 2 leaves a gap in the age-depth model. This led to the decision to send two more samples of terrestrial macrofossil origin for a precise ^{14}C dating.

As the proxies analysed in this Thesis did not reflect a climate signal, another further work recommended for this thesis would be to search for a proxy that is sensitive to a climate signal and not to eutrophication.

In order to have a deeper knowledge about the land-use changes and their effects, several other type of analysis could be attempted. Proxies that could give a better understanding of the fire regimes and vegetation changes such as charcoal and pollen counts could be studied. In addition, investigation of biological proxies such as chironomids and diatoms could give a better understanding of past changes in eutrophic conditions. To complement this, looking at persistent organic pollutants (POPs) as well as nitrogen isotopes ($\delta^{15}N$) would give a better understanding of the fertilization processes.

In order to find the sources of the volcanic tephras, a detailed geochemical profile using an inductively coupled plasma mass spectometry (ICP-MS) analysis could be used to identify their composition. After this, the tephra could be identified with its volcanic source and could be used as a temporal marker to improve the age-depth model.

7. Acknowledgments

First I would like to thanks to my supervisor Prof. Dr. Martin Grosjean for gave me the opportunity of doing this Master and work with him. I also thanks to my co-supervisor Dr. Iván Hernández Almeida, for his always good disposition to help me and try to solve any problem that arise and his good advices.

I thank to Dr. Daniela Fischer, for all her help in the lab work, her infinite patience when she try to teach me a new lab procedure, and for those very nice talks about the Chilean Patagonia. To my lab colleagues: Tobias, Alena, Krystyna, Christoph, Martin (Schmidt), Valentin, Rixt, Iván, and Ben, for the interesting discussions about my results and for excellent coffee breaks. To my colleagues in Chile: Dr. Roberto Urrutia and Denisse Alvarez, for the support during fieldwork and to Sr. Fernando Torrejon, for the valuable historical information that he gave me.

Many thanks to everyone who contribute to thi thesis, Dr. Sönke Szidat from the Department of Chemistry and Biochemistry, Uni Bern, for the ^{137}Cs and ^{14}C measurments; Dr. Flavio Anselmetti from the Institute of Geological Science, Uni Bern, for the Geotek and XRF scanner and Christoph Butz from Group of Paleolimnology and Lake Sediments, Uni Bern, for the Specim scanner.

To my friends: Tais and Rodrigo, for being very helpful and supported in the moments of homesick. Also to my friends in Chile: Denisse and Caro, for call me during the night and have great talks about life and make me feel that I was there with you. To my family, especially to my Mom and Dad, for be there when I need them and for always support me no matters what. I would like to give special thanks to my boyfriend Pablo for support me in this adventure: it has been hard to be separated, but it worth it. Finally to all of you that form part of this adventure during my stay in Switzerland, you all will be part of my life and always remember you.

8. References

Amann, B., Lobsiger, S., Tylman, W., Filipiak, J., & Grosjean, M. (in Review). Spring temperature variability and eutrophication history inferred from sedimentary pigments in the varved sediments of Lake Zabinskie, northeast Poland, 1907-2008 AD. *Global and Palnetary Change*.

Appleby, P. G., & Oldfield, F. (1978). The calculation of ^{210}Pb dates assuming a constant rate of supply of unsuported ^{210}Pb to the sediment. *Catena*, *5*, 1–8.

Araneda, A., Jana, P., Ortega, C., Torrejón, F., Bertrand, S., Vargas, P., Fagel, N., Alvarez, D., Stehr, A., & Urrutia, R. (2013). Changes in sub-fossil chironomid assemblages in two Northern Patagonian lake systems associated with the occurrence of historical fires. *Journal of Paleolimnology*, *50*(1), 41–56. doi:10.1007/s10933-013-9703-0

Arnaud, F., Magand, O., Chapron, E., Bertrand, S., Boës, X., Charlet, F., & Mélières, M. -a. (2006). Radionuclide dating (^{210}Pb, ^{137}Cs, ^{241}Am) of recent lake sediments in a highly active geodynamic setting (Lakes Puyehue and Icalma—Chilean Lake District). *Science of The Total Environment*, *366*(2-3), 837–850. doi:10.1016/j.scitotenv.2005.08.013

Battarbee, R. W., & Bennion, H. (2010). Palaeolimnology and its developing role in assessing the history and extent of human impact on lake ecosystems. *Journal of Paleolimnology*, *45*(4), 399–404. doi:10.1007/s10933-010-9423-7

Bertrand, S., Charlet, F., Charlier, B., Renson, V., & Fagel, N. (2007). Climate variability of southern Chile since the Last Glacial Maximum: a continuous sedimentological record from Lago Puyehue (40°S). *Journal of Paleolimnology*, *39*(2), 179–195. doi:10.1007/s10933-007-9117-y

Bertrand, S., Sterken, M., Vargas-Ramirez, L., De Batist, M., Vyverman, W., Lepoint, G., & Fagel, N. (2010). Bulk organic geochemistry of sediments from Puyehue Lake and its watershed (Chile, 40°S): Implications for paleoenvironmental reconstructions. *Palaeogeography, Palaeoclimatology, Palaeoecology*, *294*(1-2), 56–71. doi:10.1016/j.palaeo.2009.03.012

Blaauw, M. (2010). Methods and code for "classical" age-modelling of radiocarbon sequences. *Quaternary Geochronology*, *5*(5), 512–518. doi:10.1016/j.quageo.2010.01.002

Boyle, J. F. (2001). Inorganic Geochemical Methods in Paleolimnology. In W. M. Last & J. P. Smol (Eds.), *Tracking Environmental Change Using Lake Sediments. Volume 1: Basin Analysis, Coring, and Chronological Techniques* (Vol. 2, pp. 83–141). Dordrecht: Kluwer Academic Publishers.

Cohen, A. S. (2003). *Paleolimnology: The history and Evolution of Lake System* (p. 500). New York: Oxford University Press.

Conley, D. J., & Schelske, C. L. (2001). Biogenic silica. In W. M. Last & J. P. Smol (Eds.), *Tracking Environmental Change Using Lake Sediments. Volume 3: Terrestrial, algal, and Siliceous Indicators* (pp. 281–294). Dordrecht: Kluwer Academic Publishers.

Dillehay, T. (1990). *Araucanía: Presente y Pasado.* (p. 153). Santiago de Chile: Editorial Andrés Bello.

ENVI 5.0 (Exelis Visual Information Solutions, Boulder, Colorado).

FAO. (2006). *Livestock's long shadow: environmental issues and options* (p. 416). Rome, Italy: FAO.

Fletcher, M.-S., & Moreno, P. I. (2012). Vegetation, climate and fire regime changes in the Andean region of southern Chile (38°S) covaried with centennial-scale climate anomalies in the tropical Pacific over the last 1500 years. *Quaternary Science Reviews*, *46*, 46–56. doi:10.1016/j.quascirev.2012.04.016

Fontijn, K., Lachowycz, S. M., Rawson, H., Pyle, D. M., Mather, T. A., Naranjo, J. A., & Moreno-roa, H. (2014). Late Quaternary tephrostratigraphy of southern Chile and Argentina. *Quaternary Science Reviews*, *89*, 70–84. doi:10.1016/j.quascirev.2014.02.007

Garreaud, R. D., Vuille, M., Compagnucci, R., & Marengo, J. (2009). Present-day South American climate. *Palaeogeography, Palaeoclimatology, Palaeoecology*, *281*(3-4), 180–195. doi:10.1016/j.palaeo.2007.10.032

Håkanso, L., & Jansson, M. (2002). *Principles of Lake Sedimentology* (2° ed., p. 316). Caldwell, New Yersey: The Blackburn Press.

Hennekam, R., & Lange, G. De. (2012). X-ray fluorescence core scanning of wet marine sediments : methods to improve quality and reproducibility of high- resolution paleoenvironmental records. *Limnology and Oceanography: Methods*, *10*, 991–1003. doi:10.4319/lom.2012.10.991

Hogg, A., Hua, Q., & Blackwell, P. (2013). SHCal13 Southern Hemisphere Calibration, 0-50,000 years cal BP. *Radiocarbon*, *55*(4), 1889–1903.

IPCC. (2013). *The Physical Science Basis. Contribution of Working Group I to the Fifth Assessment Report of the Intergovern- mental Panel on Climate Change*. (T. F. Stocker, S. K. Allen, V. Bex, & P. M. Midgley, Eds.) (p. 1535). Cambridge, United Kingdom and New York, NY, USA,: Cambridge University Press.

Jolliffe, I. (1987). Principal component analysis. *Chemometrics and Intelligent Laboratory Systems*, *2*(1-3), 37–52. doi:10.1016/0169-7439(87)80084-9

Koroluk, S. L., & de Boer, D. H. (2007). Land use change and erosional history in a lake catchment system on the Canadian prairies. *Catena*, *70*(2), 155–168. doi:10.1016/j.catena.2006.08.006

Kylander, M. E., Ampel, L., Wohlfarth, B., & Veres, D. (2011). High-resolution X-ray fluorescence core scanning analysis of Les Echets (France) sedimentary sequence : new insights from chemical proxies, *26*, 109–117. doi:10.1002/jqs.1438

Mann, M. E., Zhang, Z., Hughes, M. K., Bradley, R. S., Miller, S. K., Rutherford, S., & Ni, F. (2008). Proxy-based reconstructions of hemispheric and global surface temperature variations over the past two millennia. *Proceedings of the National Academy of Sciences of the United States*, *105*(36), 13252–7. doi:10.1073/pnas.0805721105.

McWethy, D. B., Whitlock, C., Wilmshurst, J. M., McGlone, M. S., Fromont, M., Li, X., Dieffenbacher-Krall, A., Hobbs, W. O., Fritz, S. C., & Cook, E. R. (2010). Rapid landscape transformation in South Island, New Zealand, following initial Polynesian settlement. *Proceedings of the National Academy of Sciences of the United States*, *107*(50), 21343–8. doi:10.1073/pnas.1011801107

Mees, F., Swennen, R., Geet, M. V., & Jacobs, P. (2003). Applications of X-ray computed tomography in the geosciences. *Geological Society, London, Special Publications*, *215*(1), 1–6. doi:10.1144/GSL.SP.2003.215.01.01

Meyers, P. A., & Teranes, J. L. (2001). Sediment Organic Matter. In U. of M. Last, William M. (Department of Geological Sciences & Q. U. Smol, John P. (Department of Biology (Eds.),

Tracking Environmental Change Using Lake Sediments. Volume 2: Physical and Geochemical Methods (Vol. 2, pp. 239–269). Dordrecht: Kluwer Academic Publishers.

Montecinos, A., Díaz, A., & Aceituno, P. (2000). Seasonal Diagnostic and Predictability of Rainfall in Subtropical South America Based on Tropical Pacific SST. *Journal of Climate*, *13*(4), 746–758. doi:10.1175/1520-0442(2000)013<0746:SDAPOR>2.0.CO;2

Naeher, S., Gilli, A., North, R. P., Hamann, Y., & Schubert, C. J. (2013). Tracing bottom water oxygenation with sedimentary Mn/Fe ratios in Lake Zurich, Switzerland. *Chemical Geology*, *352*, 125–133. doi:10.1016/j.chemgeo.2013.06.006

Neukom, R., Luterbacher, J., Villalba, R., Küttel, M., Frank, D., Jones, P. D., Grosjean, M., Wanner, H., Aravena, J. C., Black, D. E., Christie, D. A., D'Arrigo, R., Lara, A., Morales, M., Soliz-Gamboa, C., Srur, A., Urrutia, R., & von Gunten, L. (2011). Multiproxy summer and winter surface air temperature field reconstructions for southern South America covering the past centuries. *Climate Dynamics*, *37*, 35–51. doi:10.1007/s00382-010-0793-3

Otero, L. (2006). *La huella del fuego: Historia de los bosques nativos, poblamiento y cambios en el paisaje del Sur de Chile.* (p. 171). Santiago de Chile: Pehuen.

Pankhurst, R. J., & Hervé, F. (2007). Introduction and overview. In T. Moreno & W. Gibbson (Eds.), *The Geology of Chile* (pp. 1–4). London, England: The Geological Society of London.

Pfeiffer, T., Costa, a., & Macedonio, G. (2005). A model for the numerical simulation of tephra fall deposits. *Journal of Volcanology and Geothermal Research*, *140*(4), 273–294. doi:10.1016/j.jvolgeores.2004.09.001

R Core Team. (2012). R: A language and environment for statistical computing. Vienna, Austria: R Foundation for Statistical Computing. Retrieved from http://www.r-project.org/

Rein, B., & Sirocko, F. (2002). In-situ reflectance spectroscopy - analysing techniques for high-resolution pigment logging in sediment cores. *International Journal of Earth Sciences*, *91*(5), 950–954. doi:10.1007/s00531-002-0264-0

Sandgren, P., & Snowball, I. (2001). Application of Mineral Magnetic Techniques to Paleolimnology. In W. M. Last & J. P. Smol (Eds.), *Tracking Environmental Change Using Lake Sediments. Volume 2: Physical and Geochemical Methods* (Vol. 2, pp. 217–237). Dordrecht: Kluwer Academic Publishers.

Schnurrenberger, D., Russell, J., & Kelts, K. (2003). Classification of lacustrine sediments based on sedimentary components. *Journal of Paleolimnology*, *29*, 141–154.

Smol, J. P. (2008). *Pollution of Lakes and Rivers* (Second., p. 383). Malden: Blackwell Publising.

Stern, C. R., Moreno, H., Lopez-Escobar, L., Clavero, J. E., Lara, L. E., Naranjo, J. A., Parada, M., & Skewes, M. A. (2007). Chilean Volcanoes. In T. Moreno & W. Gibbons (Eds.), *The Geology of Chile* (pp. 147–178). London, England: The Geological Society of London.

Stern, R. C., & Naranjo, J. A. (1998). Holocene explosive activity of Hudson Volcano , southern Andes. *Bulletin of Volcanology*, *59*, 291–306.

Sveinbjornsdottir, A. E., Heinemeier, J. A. N., & Johnseni, S. J. (1992). Growing in icelandic radiocarbon anomalies observed for plants geothermal waters. *Radiocarbon*, *34*(3), 696–703.

Torrejón, F., & Cisternas, M. (2002). Alteraciones del paisaje ecológico araucano por la asimilación mapuche de la agroganadería hispano-mediterránea (siglos XVI y XVII). *Revista Chilena de Historia Natural*, *75*, 729–736.

Trouet, V., & van Oldenborgh, G. (2013). KNMI Climate Explorer: a web-based research tool for high-resolution paleoclimatology. *Tree-Ring Research*, *69*(1), 3–13. Retrieved from http://www.bioone.org/doi/abs/10.3959/1536-1098-69.1.3

Van Hengstum, P. J., Reinhardt, E. G., Boyce, J. I., & Clark, C. (2007). Changing sedimentation patterns due to historical land-use change in Frenchman's Bay, Pickering, Canada: evidence from high-resolution textural analysis. *Journal of Paleolimnology*, *37*(4), 603–618. doi:10.1007/s10933-006-9057-y

Verniory, G. (2001). *Diez años en Araucanía: 1889-1899* (2° ed., p. 493). Santiago de Chile: Pehuen.

Vogel, H., Wagner, B., Zanchetta, G., Sulpizio, R., & Rosen, P. (2010). A paleoclimate record with tephrochronological age control for the last glacial-interglacial cycle from Lake Ohrid, Albania and Macedonia. *Journal of Paleolimnology*, *44*, 295–310. doi:10.1007/s10933-009-9404-x

Von Gunten, L., Grosjean, M., Kamenik, C., Fujak, M., & Urrutia, R. (2012). Calibrating biogeochemical and physical climate proxies from non-varved lake sediments with meteorological data : methods and case studies. *Journal of Paleolimnology*, *47*, 583–600. doi:10.1007/s10933-012-9582-9

Von Gunten, L., Grosjean, M., Rein, B., Urrutia, R., & Appleby, P. (2009a). A quantitative high-resolution summer temperature reconstruction based on sedimentary pigments from Laguna Aculeo, central Chile, back to AD 850. *The Holocene*, *19*(6), 873–881. doi:10.1177/0959683609336573

Von Gunten-b, L., Grosjean, M., Beer, J., Grob, P., Morales, A., & Urrutia, R. (2009b). Age modeling of young non-varved lake sediments: methods and limits. Examples from two lakes in Central Chile. *Journal of Paleolimnology*, *42*(3), 401–412. doi:10.1007/s10933-008-9284-5

Weltje, G. J., & Prins, M. a. (2007). Genetically meaningful decomposition of grain-size distributions. *Sedimentary Geology*, *202*(3), 409–424. doi:10.1016/j.sedgeo.2007.03.007

Zolitschka, B., Mingram, J., van der Gaast, S., Jansen, J. H. F., & Naumann, R. (2001). Sediment logging techniques. In W. M. Last & J. P. Smol (Eds.), *Tracking Environmental Change Using Lake Sediments. Volume 1: Basin Analysis, Coring, and Chronological Techniques* (pp. 137–154). Dordrecht: Kluwer Academic Publishers.

Declaration

under Art. 28 Para. 2 RSL 05

Last, first name: Jana Pinninghoff, Patricia Alejandra

Matriculation number: 12-103-826

Programme: Master in Climate Sciences

Bachelor ☐ Master ☒ Dissertation ☐

Thesis title: Climatic and Environmental History of the Past 1700 years Recorded in the sediments of Laguna Espejo (39˚S) South-Central Chile.

Thesis supervisor: Prof. Dr. Martin Grosjean

I hereby declare that this submission is my own work and that, to the best of my knowledge and belief, it contains no material previously published or written by another person, except where due acknowledgement has been made in the text. In accordance with academic rules and ethical conduct, I have fully cited and referenced all material and results that are not original to this work. I am well aware of the fact that, on the basis of Article 36 Paragraph 1 Letter o of the University Law of 5 September 1996, the Senate is entitled to deny the title awarded on the basis of this work if proven otherwise.

.....

Place, date

.....

Signature